1-1-2015

On Thermal Aging Prevention in Polymer Core Composite Conductor Rods

Joe D. Hoffman
University of Denver

ON THERMAL AGING PREVENTION IN POLYMER CORE COMPOSITE CONDUCTOR RODS

_____

A Dissertation

Presented to

The Faculty of the Daniel Felix Ritchie School of Engineering and Computer Science

University of Denver

_____

In Partial Fulfillment

Of the Requirements for the Degree

Doctor of Philosophy

_____

By

Joseph D. Hoffman

November 2015

Advisor: Dr. Maciej Kumosa

Author: Joseph D. Hoffman
Title: On Thermal Aging Prevention in Polymer Core Composite Conductor Rods
Advisor: Dr. Maciej Kumosa
Degree Date: November 2015

ABSTRACT

Increased energy usage in the United States and worldwide is driving the demand for new technologies to transmit electrical power in greater quantities and with reliable, safe, and more efficient methods. One recent innovation is to replace the standard Aluminum Conductor Steel Reinforced electrical transmission conductor with a new conductor design that utilizes a fiber reinforced polymer core rod to support a fully annealed aluminum conductor. This new technology that includes a hybrid carbon fiber/epoxy and glass fiber/epoxy support core allows for better efficiency and for greater current to be transmitted in the same size and weight line. These new conductor lines are part of a new class of conductors called High Temperature Low Sag (HTLS) for their ability to transmit more current while still providing appropriate ground clearance over vegetation. However, long-term exposure to high temperatures can diminish the flexural properties of the hybrid composite core rods.

This dissertation contributes unique and innovative multiscale approaches to understand and reduce the impact of thermal aging on the core rods. The research demonstrates that the source of flexural failure in the rods moves from predominantly physical aging to predominantly chemical aging as a function of time and temperature, a brand new explanation that is validated both experimentally and numerically. Further, for the first time, it is shown that coating the rods with a barrier that may delay thermal

oxidation is an effective method of reducing and delaying chemical aging and therefore can be a practical method for increasing their service life. It also finds that while the detrimental impact of physical aging escalates with increasing temperature as expected, the effect of chemical aging is in fact mitigated by moving from aging at 180 °C to 200 °C. In addition, the dissertation evaluates the benefit of increasing radiative cooling on the operating temperature of the conductor in order to find a method of transmitting the same current while reducing the thermal aging. Lastly, the impact of incorporating nanoparticles into the epoxy matrix is assessed to identify an additional method of retarding thermal aging.

Thus, instead of simply identifying and explaining problems, this research goes a step further and offers a comprehensive approach to preventing thermal aging of the conductors and other structures utilizing polymer matrix composites. It offers significant advances in the use of nanotechnology to reduce aging of polymer composites; it identifies a coating to reduce the impact of chemical aging; and it suggests a radiative cooling as an important approach to reduce both physical and chemical aging in the rods. All of these tactics are evaluated both experimentally and numerically in this work. Most importantly, this research advances the understanding and improves the performance of polymer core HTLS conductors along with other polymer composites subjected to high temperatures. With the improvement and adoption of the techniques presented, confidence in the safety and endurance of the novel conductor is increasing its implementation in this country and around the world.

ACKNOWLEDGEMENTS

Performing research to create a thesis is generally not a task performed in isolation and the work for this dissertation was no exception. I relied upon the prior work, support, insights, and help from many other researchers, especially those in Dr. Kumosa's lab. My research built upon prior studies performed by Dr. Brian Burks and Dr. James Middleton and I relied on Eva Hakansson for her help in designing tests and Dr. Euripides Solis-Ramos for his support of my SEM work.. I would also like to thank the members of my Committee who were also my teachers and mentors across the years. Most of all, I would like to thank Dr. Kumosa for his tireless academic support and his continuous financial support. He offered his perseverance, his energy, and his (way) out-of-the-box thinking and I cannot thank him enough for his encouragement and patronage.

On the financial side, I would like to thank my original sponsors, Western Area Power Association, Bonneville Power Association, and Tri-State Generation and Transmission, and the National Science Foundation under GOALI grant #1232520 and I/UCRC grant #1362135. I would also like to thank the National Science Foundation Center for Novel High Voltage/Temperature Materials and Structures E.L.Stone Company, Cabot Corporation, Lindau Chemical, Composites Technology Development, and CTC Global. Along with the researchers at MTU, especially Dr. Julie King and Dr. Danielle Klimek-McDonald .

And lastly I would like to thank my wife, Deb, and my children, Sam, Becca, and Abe, who provided great encouragement and did not ask me (too often) when I would be done.

TABLE OF CONTENTS

LIST OF TABLES

LIST OF FIGURES

CHAPTER 1 INTRODUCTION

New High Temperature Low Sag Conductors (HTLS) offer several benefits over standard Aluminum Conductor Steel Reinforced (ACSR) electrical transmission lines [1,2]. First, HTLS conductors have a stronger and lighter core which can fully support the line and can therefore use a lower mechanical strength annealed aluminum as the conductive material. Fully annealed aluminum has lower resistance than the aluminum used in ACSR lines and thus transmits power with lower line losses. Secondly, HTLS conductors are capable of running at higher temperatures, allowing more power to be run through the same diameter lines, reducing the need to add additional or stronger towers. The low sag nature of the lines allows the lines to be run at high temperatures while still maintaining required ground and vegetation clearance which is now a federal requirement in the United States.

There are several types of HTLS conductors. Some examples are Polymer Core Composite Conductors (PCCC) which use Polymer Matrix Composite (PMC) core rods and Aluminum Conductor Composite Reinforced (ACCR) which use Metal Matrix Composite (MMC) strands based on alumina fibers in an aluminum matrix as the core. One manufacturer of PCCC conductors is CTC Global which offers the Aluminum Conductor Composite Core (ACCC®) conductor. This conductor has a hybrid core with a unidirectional carbon fiber epoxy composite inner core for strength surrounded by a

unidirectional glass fiber epoxy composite that serves as a galvanic reaction barrier (see Figure 1-1). The carbon fiber volume fraction is 69% and the glass fiber volume fraction is 64% [3]. Because of the prior mentioned advantages, the manufacturer states that 2-3x the amount of power can be transmitted in the same size and weight line. In order to reach this level of transmission, however, the conductor must be run at a high temperature. The manufacturer has indicated that the conductor can be run at up to 180 ^{0}C for long periods of time [1].

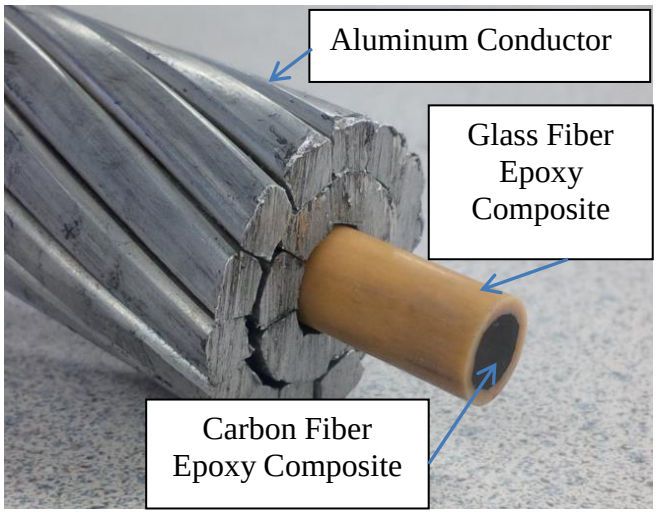

Figure 1-1. Aluminum Conductor Composite Core (ACCC®)

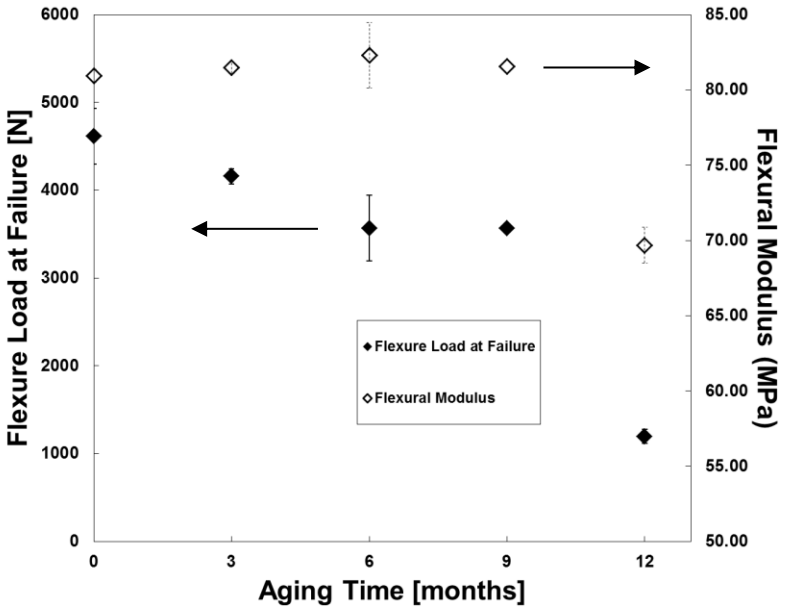

Figure 1-2. Flexure Load at Failure and Flexural Modulus of uncoated rods aged at 180 °C in air. Data courtesy of Burks et al [4].

Barjasteh et al [3] found that while there was surface oxidation present in the ACCC rods after thermal aging, tensile strength was little affected by aging at 180 ^{0}C or 200 ^{0}C for up to one year. However, Burks et al [4] found that there was a significant reduction in flexural strength and flexural modulus of the same ACCC rods due to thermal aging in air at 180 ^{0}C for one year (see Figure 1-2). Burks et al [4] found a significant reduction in fatigue properties. Decreases of 20 - 30% in the number of cycles to failure for high cycle fatigue after 6 months of 180 ^{0}C exposure were attributed to surface oxidation; reductions of about 90% after 12 months of 180 ^{0}C exposure were attributed to physical aging leading to fiber matrix interface degradation.

Recently Middleton et al [5] showed that there were no reductions in mechanical properties of the rods due to exposure to high concentrations of ozone at both room

temperature and at 140 °C. In a different study, Middleton et al [6] used a finite element model to demonstrate that residual stresses from physical aging in the hybrid composite core increase significantly with extended thermal aging at temperatures of 180 ^{0}C and above. In this same paper, Middleton et al indicated that experimental results showed there was no significant reduction of flexural strength or modulus after 12 months of aging at 140 ^{0}C. They also found that the composite rods experience postcure when first exposed to high temperatures. The rods are manufactured in a pultrusion process which limits the amount of time for the curing cycle. Thus for the first 3 months of aging at 180 ^{0}C, there would be a postcure process and the stiffness of the rods would increase [6,7].

After curing of a thermoset such as epoxy, the polymer is not in a state of equilibrium; instead there is additional free volume caused by random orientations of the polymer chains locked in during the cooldown after curing. Over time, the chains realign, relaxing the polymer to a lower energy state, reducing free volume, and producing volumetric shrinkage [8,9]. Below the glass transition temperature (T_g), an activation energy is needed to allow for this reorientation of the polymer chains and higher temperatures lead to a faster reduction in free volume. This phenomenon is called physical aging and is better described by Odegard et al [8] and Struik [9]. Physical aging does not lead to chemical changes or breaking of bonds in the polymer chain. On the other hand chemical aging through oxidation does lead to chain scission through the breaking of covalent chemical bonds [10]. Chemical aging also requires an activation energy to begin the process and higher temperatures lead to more diffusion of oxygen

into the matrix. As noted in [3] and [4] significant surface damage to the ACCC rods is caused by chemical oxidation.

This dissertation explores several method of reducing the impact of thermal aging on PCCCs. To reduce the chemical aging or surface damage, a proprietary fluorinated ethylene propylene (FEP) based coating was applied to the surface. The beneficial impact of having such a barrier is discussed in Chapter 2. In Chapter 3, the effects of aging at 200 °C are compared to those from aging at 180 °C and a surprising result is reported about the impact of higher temperatures on thermal oxidation.

Thermal aging can also be controlled by limiting the operating temperature of the conductor. Simply reducing the transmitted current load would achieve this result, but that would erase one of the benefits of these new modern conductors. Chapter 4 explores a different alternative: applying a surface coating to the entire conductor to improve its radiative cooling.

Another approach to reducing thermal aging is through the incorporation of nanoparticles into the epoxy matrix to reduce the rate of physical aging that occurs in the matrix. There have been many studies of the impact of various types of nanoparticles on the thermal and mechanical properties of assorted epoxy resins. Chapter 5 is a detailed review of the results of these studies. Due to the numerous types of nanoparticles, differences within a class of nanoparticles such as size or porosity, assorted dispersion approaches, concentration levels, and other factors, the results examined in this review were not always consistent. Additionally, not many studies deal with high temperature

cycloaliphatic epoxies that are used in ACCC conductors and other types of high temperature and high voltage applications.

Based on generalizations derived from the literature review, three specific nanoparticles were determined to be the best candidates for achieving a reduction in physical aging while still preserving important mechanical properties that are critical for the use of the epoxy matrix in a high temperature low sag conductor. The three selected nanoparticles were silica, graphene, and carbon black. The results of incorporating these three types of nanoparticles are presented in Chapter 6.

Chapter 7 explores the use of quantum chemistry utilizing ab initio models to understand the interaction between the epoxy, the curing agent, and nanoparticles. Specifically, this chapter discussed the potential of bonding reactions occurring between graphene nanoparticles, a cycloaliphatic epoxy, and the nadic methyl anhydride (NMA) hardener.

CHAPTER 2 EFFECT OF A SURFACE COATING ON FLEXURAL PERFORMANCE OF THERMALLY AGED HYBRID GLASS/CARBON EPOXY COMPOSITE RODS

2.1 Introduction

Polymer Core Composite Conductors (PCCCs) are subjected in-service to thermal aging which in some cases can be severe. To reduce aging a proprietary fluorinated ethylene propylene (FEP) based surface coating was applied to a hybrid glass/carbon epoxy composite rod used in Aluminum Core Composite Conductors (ACCC®), one type of PCCC. The rods were aged in air at 180 ^{0}C for up to 12 months. Surface damage was evaluated using optical and scanning electron microscopes and compared to uncoated rods previously subjected to the same conditions. Subsequently the rods were tested under four point bending to determine their flexural performances as a function of aging time. It was found that the uncoated rods lost significantly more flexural stiffness and strength than the coated rods. To explain the experimental mechanical results a Finite Elements Modeling (FEM) analysis was performed. A new hypothesis is offered to explain the strongly beneficial effect of the coating in maintaining mechanical properties after thermal aging. Thus it appears that FEP or other coatings could be used to significantly reduce thermal aging of glass/carbon epoxy composites and in particular extend the life of PCCCs in service.

2.2 Experimental and Numerical Procedures

2.2.1 Materials

ACCC rods were received from Western Area Power Administration (WAPA) in approximately five foot sections with the aluminum conductor still in place. Core rods were carefully removed and cleaned with acetone before being sent to a company with coating expertise, E.L. Stone. E.L. Stone lightly sandblasted the rods and coated them with a proprietary Fluorinated Ethylene Propylene (FEP) epoxy coating (see Figure 2-1). The uncoated rods have an outer diameter of 9.53 mm with the carbon fiber composite section having a diameter of approximately 6.80mm. The coating was approximately 25 microns thick. No visible damage to the fibers was evident on the surface of the rods (see Figure 2-2), even under 100x magnification.

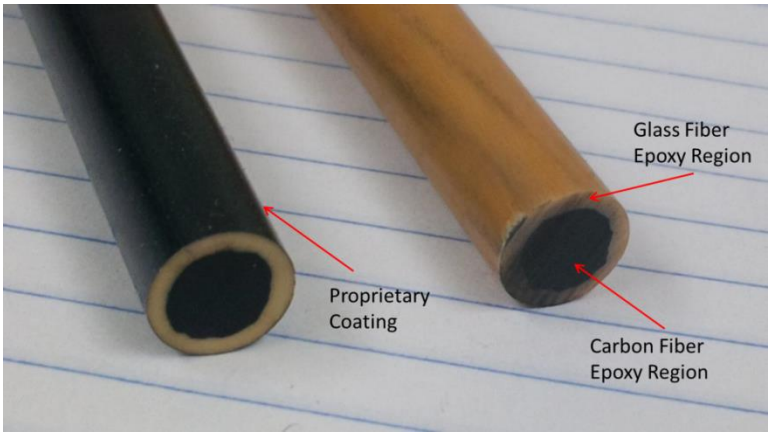

Figure 2-1. FEP Coated (left) and Uncoated (right) ACCC composite rods.

The ends of the rods were capped with a high temperature RTV sealant to prevent longitudinal oxidation. The rods were then aged in an Econotherm Laboratory Oven at 180 ^{0}C in atmospheric conditions for 3, 6, 9 and 12 months. Ramping up to aging temperature and down from the aging temperature was done at 5 ^{0}C per minute to avoid thermal shock.

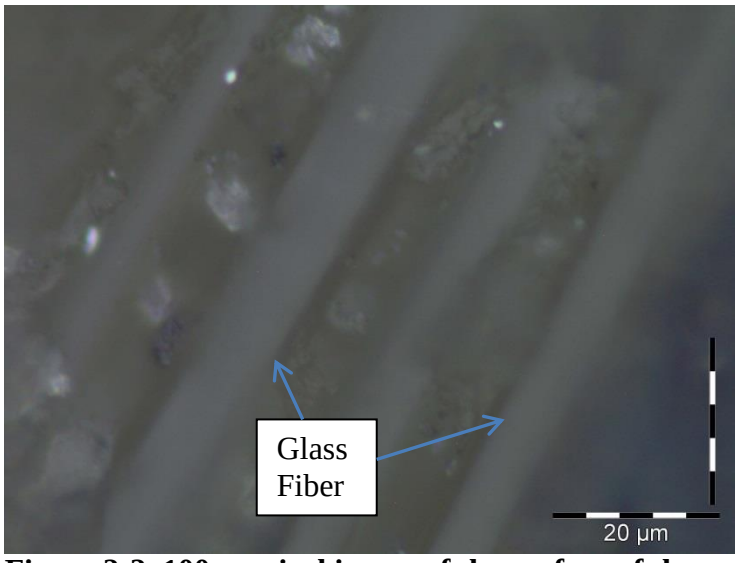

Figure 2-2. 100x optical image of the surface of the unaged coated rods, showing no damage to glass fibers.

2.2.2 Testing conditions

The rods were tested in a four-point bend test fixture custom built by Burks et al [4] in an MTS 858 test frame (see Figure 2-3). The bottom support pins were 203 mm apart and the load pins were 102 mm apart. The cross head was lowered at a constant rate of 3 mm per minute. The center point vertical displacement was measured by a linear variable displacement transducer (LVDT), along with instrument readings of crosshead displacement and load. Readings were taken at 20 Hz. The rods were wrapped with Teflon tape at contact points to avoid transverse crushing, following the recommendation given in [4].

Figure 2-3. Four-point bend test apparatus.

Examinations of the rods were performed with an Olympus BX51M optical microscope as well as by a Jeol LSM-5800LV Scanning Electron Microscope (SEM).

2.2.3 Modeling

Finite Elements Modeling of the hybrid composite rods was performed using Comsol 4.3. One quarter of the rod was modeled under force boundary conditions (see Figure 2-4) and two planes of symmetry were incorporated to improve processing time. Elastic properties of the two composites (glass fiber epoxy and carbon fiber epoxy) were determined using the Mori-Tanaka approach [11,12] of the Eshelby method [13] utilizing the initial elastic properties for the glass fiber, the carbon fiber, and the epoxy indicated in Table 2-1. The resulting stiffness matrices for the epoxy carbon fiber composite (CFC)section and the epoxy glass fiber composite (GFC) section utilized in the modeling are shown in Table 2-2 and Table 2-3, respectively. The outer radius of the GFC section was 4.76 mm and the outer radius of the CFC section was 3.40 mm with perfect bonding between the 2 sections assumed. Thus there was no slippage allowed. The half-length of the rod was 102.0 mm and the load was evenly distributed across a surface that rotated

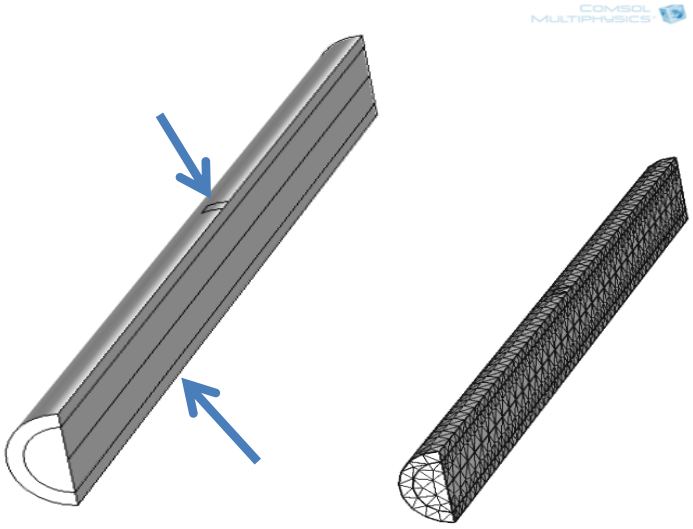

Figure 2-4. Finite Elements Model of one quarter of the hybrid composite rod with its mesh alongside. Arrows indicate load.

one eighth of the way around the half circumference (pi/8 radians) of the rod at a distance between 49 and 51 mm from the transverse symmetric plane of the rod. A fixed point at the intersection of the longitudinal axis and the transverse symmetric plane was established to eliminate translational motion. The built-in Comsol free tetrahedral meshing algorithm was used with an extremly fine setting, producing 69,706 elements.

Table 2-1. Stiffness matrix of carbon fiber, glass fiber and epoxy matrix (GPa). 3 direction is longitudinal.

$$\begin{bmatrix} 26 & 3.32 & 3.69 & 0 & 0 & 0 \\ 3.32 & 26 & 3.69 & 0 & 0 & 0 \\ 3.69 & 3.69 & 235 & 0 & 0 & 0 \\ 0 & 0 & 0 & 28.2 & 0 & 0 \\ 0 & 0 & 0 & 0 & 28.2 & 0 \\ 0 & 0 & 0 & 0 & 0 & 5.52 \end{bmatrix}$$

$$\begin{bmatrix} 86.8 & 24.5 & 24.5 & 0 & 0 & 0 \\ 24.5 & 86.8 & 24.5 & 0 & 0 & 0 \\ 24.5 & 24.5 & 86.8 & 0 & 0 & 0 \\ 0 & 0 & 0 & 31.1 & 0 & 0 \\ 0 & 0 & 0 & 0 & 31.1 & 0 \\ 0 & 0 & 0 & 0 & 0 & 31.1 \end{bmatrix}$$

$$\begin{bmatrix} 3.15 & 1.48 & 1.48 & 0 & 0 & 0 \\ 1.48 & 3.15 & 1.48 & 0 & 0 & 0 \\ 1.48 & 1.48 & 3.15 & 0 & 0 & 0 \\ 0 & 0 & 0 & 0.833 & 0 & 0 \\ 0 & 0 & 0 & 0 & 0.833 & 0 \\ 0 & 0 & 0 & 0 & 0 & 0.833 \end{bmatrix}$$

Table 2-2. Stiffness matrix of epoxy carbon fiber composite (GPa).

$$\begin{bmatrix} 9.081 & 3.238 & 2.169 & 0 & 0 & 0 \\ 3.238 & 9.081 & 2.169 & 0 & 0 & 0 \\ 2.169 & 2.169 & 163.0 & 0 & 0 & 0 \\ 0 & 0 & 0 & 6.160 & 0 & 0 \\ 0 & 0 & 0 & 0 & 6.160 & 0 \\ 0 & 0 & 0 & 0 & 0 & 2.918 \end{bmatrix}$$

Table 2-3. Stiffness matrix of epoxy glass fiber composite (GPa).

$$\begin{bmatrix} 10.05 & 4.199 & 3.555 & 0 & 0 & 0 \\ 4.199 & 10.05 & 3.555 & 0 & 0 & 0 \\ 3.555 & 3.555 & 51.21 & 0 & 0 & 0 \\ 0 & 0 & 0 & 5.373 & 0 & 0 \\ 0 & 0 & 0 & 0 & 5.373 & 0 \\ 0 & 0 & 0 & 0 & 0 & 4.608 \end{bmatrix}$$

2.3 Results and Discussion

2.3.1 Surface Characteristics

Optical images of the surface of the aged rods show a significant difference between the coated and the uncoated rods, the disparity increasing with aging time (see Figure 2-5). In the coated rods, no visible surface damage was evident for aging times up to twelve months. In the uncoated samples from [4], loose fibers were observed which became very prominent after longer than six months exposure times. SEM images of the transverse surface of the aged rods also demonstrate a marked difference. Near the surface of the aged uncoated rods, stray fibers and voids between the fibers can be observed. In the coated rods, the surface shows much less damage both under optical imaging (Figure 2-6) and SEM imaging (Figure 2-7).

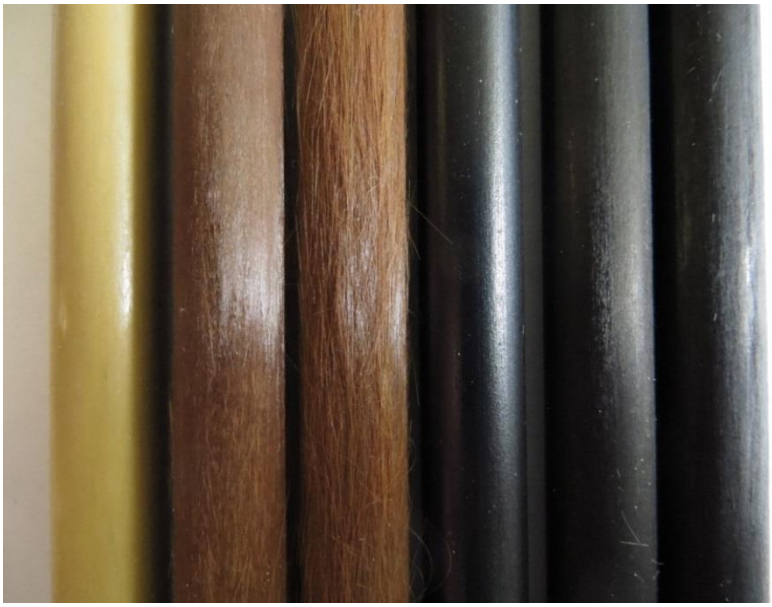

Figure 2-5. Uncoated (left) and coated rods (right) after 0, 6, and 12 months of aging.

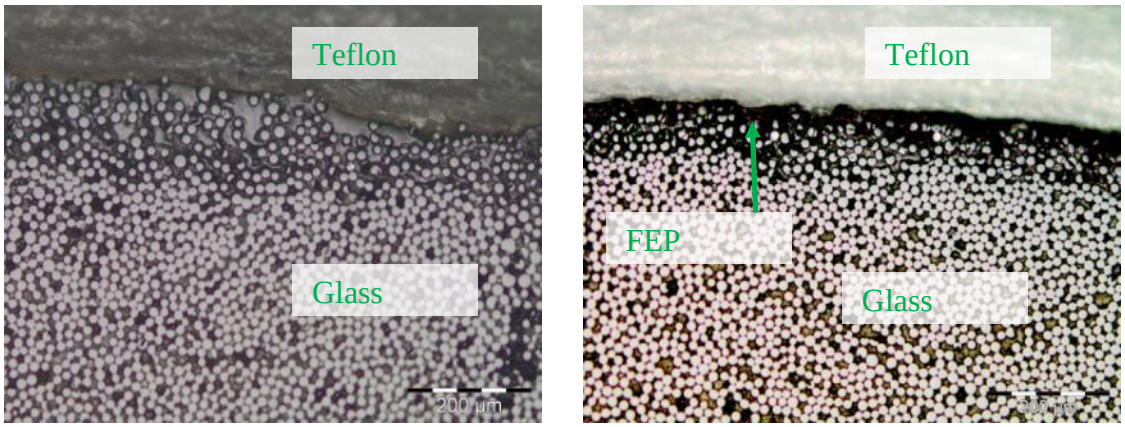

Uncoated Rod Aged 12 Months at 180 °C. 10x Magnification

FEP Coated Rod Aged 12 Months at 180 °C. 10x Magnification

Figure 2-6. Transverse optical images of the surface of the rods. Teflon tape was wrapped around rods to prevent damage during cutting and potting.

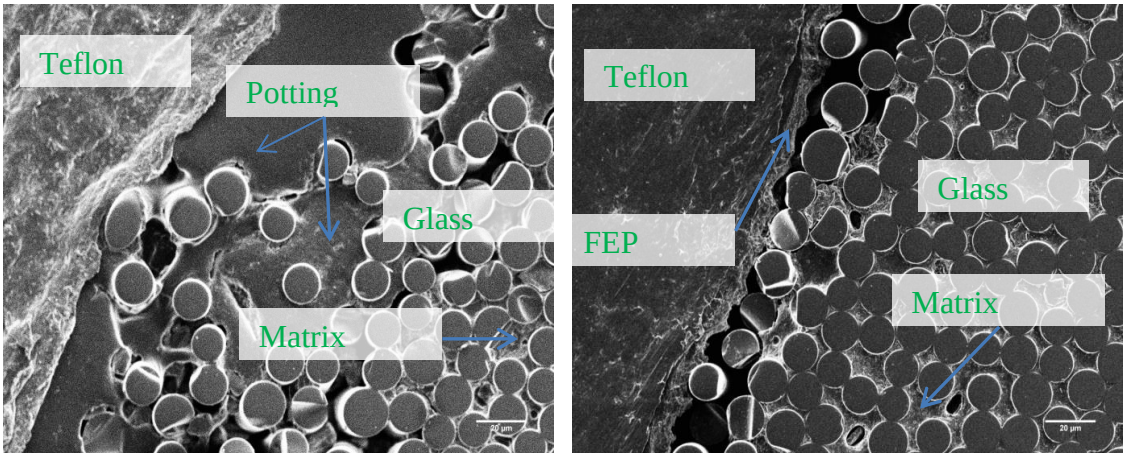

Figure 2-7. SEM Image (600x) of edge of uncoated rod (left) and coated rod (right) after 12 months of aging.

2.3.2 Four-point bend test data

In the four-point bend test, with the exception of one rod, all twenty-six coated specimens broke with a split in the horizontal mid-plane of the specimens (see Figure 2-8). This failure mode is predominantly characteristic of pure intralaminar shear failure with the effects of other stresses either entirely eliminated or at least significantly

reduced. The number of coated samples tested at 0, 3, 6, 9, and 12 months were 3, 6, 6, 6, and 5 respectively. For uncoated samples, Burks [4] tested 4, 5, 5, 2, and 5 rods for the same respective aging times.

Figure 2-8. 12 month aged rods after flexural failure. Coated (top) and uncoated (bottom).

It has been found in [4] that the flexural modulus remained relatively constant for uncoated rods after 0, 3, 6, and 9 months of aging at 180 ^{0}C, but there was a dramatic decrease of about 14% in this modulus after 12 months of aging (see Figure 2-9 and Table 2-4). For the coated rods, the result was different: the rods showed a small but steady increase in flexural modulus up through 12 months of aging at 180 ^{0}C. After 12 months of aging, the increase in the flexural modulus of the coated rods compared to the unaged samples was about 3%.

As for the flexure load at failure (see Figure 2-9), there was no significant difference between the coated and the uncoated rods before aging. For the uncoated rods, Burks et al [4] found a steady decline through 9 months of aging followed by a rapid decrease after 12. Through 9 months, the decrease was about 23%, but after 12 months

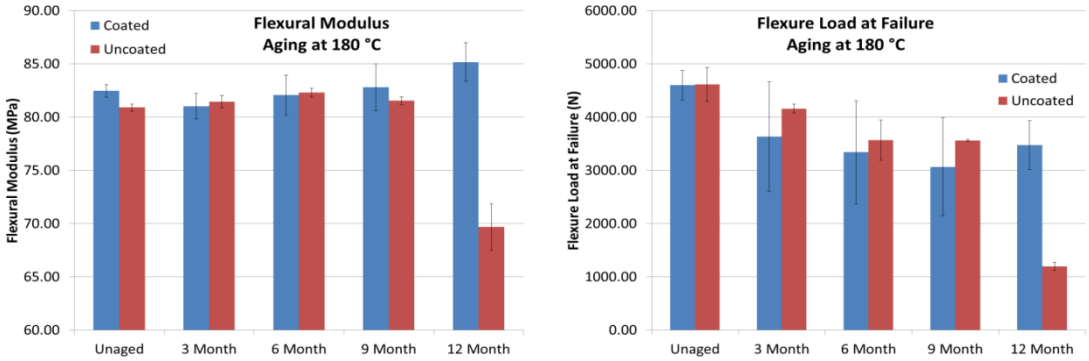

Figure 2-9. Flexural modulus (left) and load at failure (right) of coated and uncoated aged rods. Error bars are one standard deviation.

the reduction was about 74%. The coated rods showed similar reductions across the first nine months of aging. However, they only showed a decrease of about 24% even after 12 months of aging. Interestingly, in the coated rods, the load at failure did not show much change between the various aging lengths, although there was a lot of scatter in the results as indicated by the size of the error bars.

Table 2-4. Flexural property changes after aging at 180 °C in air

		Aging time in Months			
		3	6	9	12
Flexural Modulus	Uncoated	-1%	0%	-1%	-16%
	Coated	3%	3%	4%	8%
Load at Flexure Failure	Uncoated	-10%	-23%	-23%	-74%
	Coated	-21%	-27%	-33%	-24%

2.3.3 FEM results

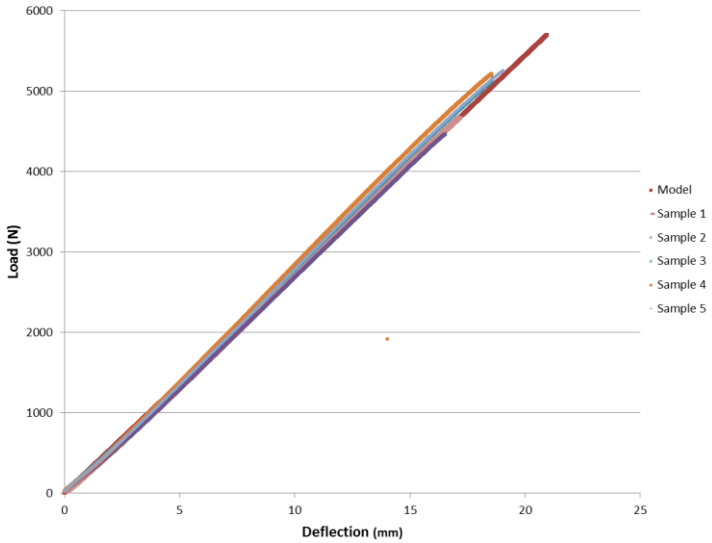

Figure 2-10. Comparison of finite elements load deflection curve versus five unaged uncoated samples tested in 4-point bend.

As a first step of the numerical analysis, the numerical load deflection diagram was compared to the experimental load deflection curves for 5 unaged samples tested in a four point bend configuration. As Figure 2-10 shows, there is a very close match between the experiments and the model, providing assurance that the FEM model was based on both the proper stiffness properties and boundary conditions. Subsequently, tensile stresses were evaluated in the rods at the rated tensile load of 153.5 kN (34.5 kip). The results shown in Figure 2-11 indicate uniform tensile stresses of 3.2 GPa in the carbon fiber region and similarly uniform but much lower tensile stresses in the glass fiber region of about 1.0 GPa in magnitude. As expected a large jump in the longitudinal

stresses was observed at the glass/carbon fiber interface. Next tensile stresses were evaluated in a 4 point bend simulation with an equivalent applied load of 4800 N, a load slightly larger than the flexure load at failure for unaged rods. Tensile stresses under bending in both the glass fiber and carbon fiber regions did not exceed the tensile stresses under axial tension, although the glass fiber region maximum tensile loads under bending were about 10% lower than at the rated tensile load (see Figure 2-12). Shear stresses in the rods were then evaluated at this same flexure load of 4800 N. As expected shear stresses were greatest in the horizontal mid-plane between the support and load pins. Shear stresses approached zero between the load pins and outside of the support pins.

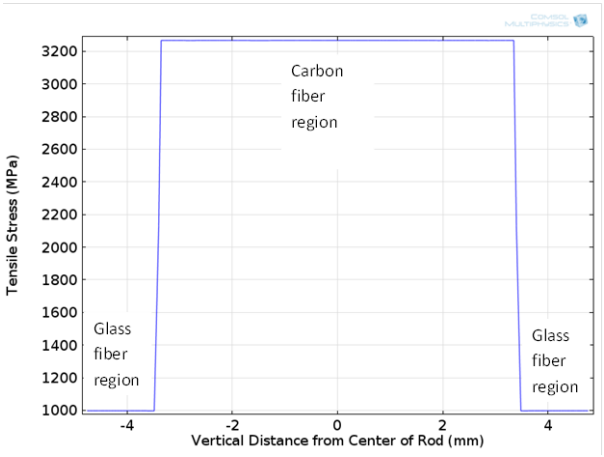

Figure 2-11. Tensile stresses in modeled rod subjected to a tensile load of 153.5 kN (the rated load).

Figure 2-13a shows the xz shear stress (x is load direction and z is longitudinal direction) along a vertical (load direction) radius in the rod at the midpoint between the support and load pins and the same

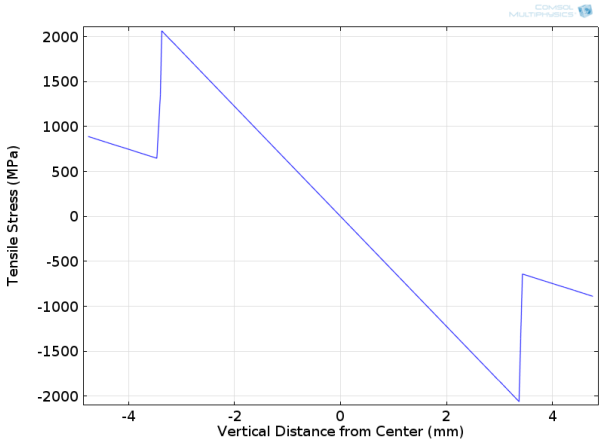

Figure 2-12. Tensile stresses along vertical (load direction) axis, in the region of maximum curvature (between load pins) in the rod subjected to flexural loading.

xz shear stress along a transverse horizontal radius in the rod at the midpoint between the support and load pins. Shear stresses are highest in the center of the rod in the carbon fiber region and diminish towards the edge. A clearly observable jump in the stresses was noticed at the glass/carbon interface along the horizontal axis. In the vertical direction (Figure 2-13b) shear stresses are zero at the top and bottom of the rod as expected. At the carbon/glass interface the stresses exhibit a small discontinuity without, however, any significant jumps.

To explore the potential impact of surface stress concentrations caused by surface

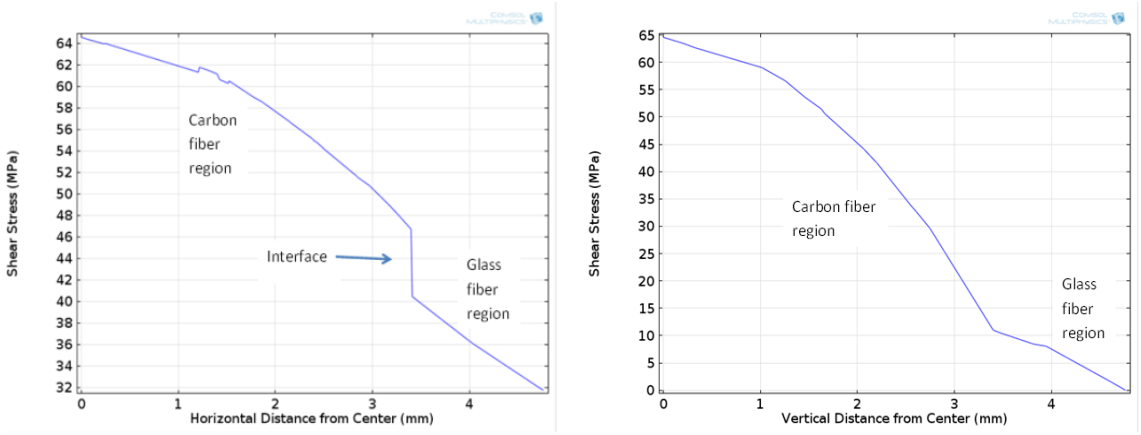

(a) (b)

Figure 2-13. Shear stresses along the load direction axis (a) and along the horizontal axis (b). Calculations conducted halfway between the support and load pins.

damage due to chemical aging, a small conical frustum shaped notch (see Figure 2-14) was then inserted into the FEM model at the edge of the rod at the end of the horizontal radius. In spite of the obvious simplicity of this surface damage model, Figure 2-15 shows a significant shear stress concentration at the surface of the notch. Other stresses are also concentrated in this location.

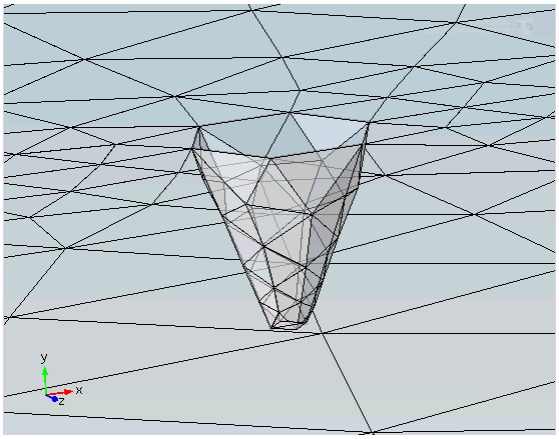

Figure 2-14. Mesh showing conical frustum shaped notch. Top radius is 5 microns, bottom radius is 1 micron and height is 10 microns.

2.3.4 Explanation of coating effect

It can be seen in Figure 2-9 and Table 2 that there is a significant difference in the mechanical performance of the coated versus the uncoated rods after 12 months of aging in atmospheric conditions at 180 ^{0}C. The uncoated rods show a dramatic decrease in flexural modulus and in flexural load at failure. While there was a steady decline in these properties during the first nine months of aging, the dropoff became dramatic between 9 and 12 months. After nine months, the rods had only lost 1% of their original flexural stiffness but after 12 months they had lost 14%. Similarly, the load at flexure failure dropped 23% after 9 months and 74% after 12 months. In contrast, the coated rods did not show this dramatic dropoff. In fact, the rods showed a somewhat steady increase in stiffness up through 12 months and the load at failure was fairly constant after 3 months of aging up through 12 months.

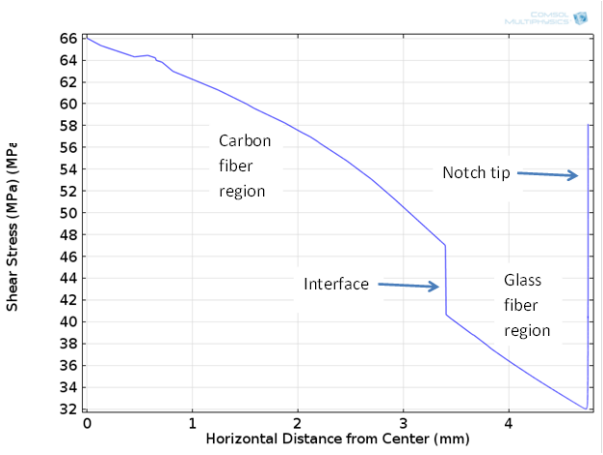

Figure 2-15. Shear stresses along a horizontal radius with a small conical frustum notch on the edge of the rod at a point halfway between the load and support pins.

The flexural property changes summarized in Table 2-4 indicate a potential change in the mechanism of failure for the 12 month aged rods between the coated and uncoated samples. There are at least three factors in play in explaining the trends in flexural strength and stiffness. It is believed that physical aging significantly increases the residual stresses in the bulk of the composite at temperatures higher than 160 °C as shown by Middleton et al [6]. This model showed that residual stresses after one year of aging at 180 °C increased by over 100%, but that they only increased by about 25% for one year of aging at 140 °C. At these higher temperatures, further crosslinking of the polymer (commonly called postcuring), occurs in the epoxy, creating a stiffer material. At the same time, on the surface, there is chemical oxidation and degradation of the epoxy matrix leading to loss of reinforcement from unconnected or partially connected fibers (see Figure 2-5). The chemical aging forms a network of surface cracks leading into the bulk of the composite (see Figure 2-7). These cracks create significant surface

stress concentrations which, if large enough, affect the overall failure process of the rods. The effect of the surface cracks on the stresses was shown in the FEM model with the surface stress concentrators.

Looking at the results presented in Figure 2-9 another significant difference can be noticed in the loads at failure between the coated and uncoated samples. The scatter in the loads for the uncoated rods is significantly smaller than in the case of the coated ones. Clearly different factors must have contributed to the process for the coated and uncoated rods. This will be further discussed later on in this section.

Burks et al [4] proposed that surface oxidation was responsible for diminished performance after 6 months of aging; however, his conclusion was that 12 months of physical aging led to the eventual breakdown of the interface between the fibers and the epoxy, an explanation supported by his observation of small amounts of matrix cracking and debonding in the bulk of the carbon/epoxy material. Based on the data presented in this chapter, an alternative hypothesis based on the three factors in play—postcuring, physical aging, and chemical aging—is offered. Postcuring, by itself, gradually increases the stiffness of the composite materials. Physical aging increases the residual stress and therefore slowly decreases the flexural strength of the composite, as indicated by the decrease in flexural load at failure for both types of the rods. Surface oxidation gradually reduces the amount of material providing mechanical support, leading to a gradual reduction in flexural stiffness and strength. This chemical aging also leads to significant surface cracks (or even damage zones consisting of numerous cracks), both on the surface and as pathways for further oxidation into the bulk material. This further reduces the

amount of material supporting the rods under bending and the creation of more and longer cracks.

In a cylindrical rod under bending, the stiffness is proportional to r^4 where r is the radius of the rod. Therefore, in a hybrid composite where only one material is eroding from the surface, the theoretical flexural modulus compared to the original hybrid modulus will be:

$$\frac{Eg * ((R')^4 - r^4) + Ec * r^4}{Eg * (R^4 - r^4) + Ec * r^4}$$

where

Eg =	47.0 GPa	Longitudinal modulus of glass fiber composite region
Ec =	139.2 GPa	Longitudinal modulus of carbon fiber composite region
R =	4.7625 mm	Original radius of hybrid rod
r =	3.3995 mm	Radius of carbon fiber region
R' =	Variable mm	Radius after surface damage/erosion

To achieve a 14% reduction in perceived flexural modulus (where no reduction in measured surface diameter is assumed, but oxidation damage has eliminated the contribution of some portion of the surface), approximately 270 microns of the glass fiber region would need to be affected. Barjasteh et al [3] found the visible thickness of the oxidation layer to be 140 microns as indicated by a color change, but did not search for additional evidence of oxidation damage deeper into the composite. In our case the uncoated rods did develop surface damage zones of the same magnitude or even larger (see Figure 2-6 and Figure 2-7).

Considering the above, for the uncoated rods, it is believed that during the first nine months of aging the roughly constant flexural stiffness is a product of the increase in stiffness from postcuring and physical aging offset by a decrease due to erosion of the surface layer from chemical aging. The strength gradually declines as residual stresses build from physical aging in the bulk material and chemical aging leads to surface damage. At some point between 9 and 12 months, the surface damage produces cracks that are significant enough both in their numbers and length to produce initiation points for shear failure leading to a change in the mode of failure from mostly physical aging dominated to mostly chemical aging dominated and a dramatic reduction in strength (see Figure 2-9). The FEM model lends support to this hypothesis as it demonstrates significant stress concentrations can form due to surface damage. It can also be assumed that the physically aging driven shear failures are less affected by other stresses than in the case of the chemical aging driven shear failures which could be affected more by normal stresses from the surface further reducing the overall loads at failure.

Since the inter/intralaminar shear strengths of both glass/epoxy and carbon/epoxy composites are higher than their transverse tensile strengths [14], any transverse tensile stresses concentrating around the surface cracks would further reduce the strength of the rods.

For the coated rods, much of the surface damage from chemical aging is eliminated even for long aging times. Thus there is an increase in stiffness (see Figure 2-9) from postcuring and physical aging with no counter effect from chemical aging. The strength is reduced from physical aging but because the coating protects against

significant surface cracks there is no change in the initiation process of shear failure so there is no dramatic change in the flexure load at failure. Thus there is no dramatic dropoff in strength of the coated rods.

The change in the modes of failure from physical aging driven (coated) to chemical aging dominated (uncoated) could also explain the differences in the scatter in the loads at failure. Both glass/epoxy and carbon/epoxy composites are brittle materials and their transverse and shear strengths are very low. In particular, in the case of the cycloaliphatic resin investigated in this study these strengths at room temperature could be low. Therefore, the coated rods could be failing similar to very brittle materials with much more scatter in the failure loads than the uncoated ones which could be failing more like ductile materials since the crack length effect would be less important.

It needs to be noted that the rods used by Burks et al [4] and the coated rods used in this experiment were not from the exact same batch of rods and it is possible that there is a slightly different matrix material (still cycloaliphatic but from a different supplier) leading to the divergent results. The coated rods were received from WAPA and were produced much earlier than the uncoated rods which Burks et al received directly from CTC Global about 4-5 years ago. However, the fact that the coated samples were from an older batch only reinforces the benefits of the coating and strengthens the most important observations obtained in this study.

2.4 Summary of Chapter 2

It has been shown in this study that coating glass/carbon/epoxy hybrid rods with a fluorinated ethylene propylene based coating provides measurable protection from thermal aging. Coated rods showed significantly better retention of flexural strength and stiffness after 12 months of aging at 180 ^{0}C in air compared to results previously observed in uncoated rods subjected to the same conditions. Visible surface damage and stray surface fibers were also eliminated as shown by surface and transverse slice optical images. A new hypothesis was offered to explain the difference in mechanical properties of the coated rods versus the uncoated rods. In the uncoated rods, physical aging dominates the reduction in flexural properties for the first nine months of thermal aging with some small offset due to postcuring. However, at some point between nine and twelve months, surface damage on the uncoated rods caused by chemical aging creates microcracks significant enough to change the dominant mode of failure. This surface damage leads to a dramatic reduction in flexural strength, a loss that is eliminated by the protection provided by the coating.

CHAPTER 3 AGING AT 200 °C

3.1 Introduction

In order to further accelerate the aging process of the hybrid composite rods, it was decided to age the rods at a higher temperature, 200 °C. Middleton et al [6] demonstrated using a finite elements model that residual stresses from physical aging would be greater at a higher temperature for a given aging duration and thus it was expected that flexural strengths would diminish more quickly for a higher temperature. The test was also conducted to see if there would also be the same dramatic dropoff in load at failure and at what aging duration that would occur.

3.2 Methods

Coated and uncoated hybrid composite rods were utilized in this experiment. The FEP coated rods were from the same batch as in the prior chapter and the uncoated rods were from the same reel from the Western Area Power Association as those that were coated. The same process of protecting the ends and aging the rods in atmospheric conditions was used as in the 180 °C aging experiment from Chapter 2, but in this case the rods were aged at 200 °C. Three samples of coated and uncoated rods were utilized at each aging time. Aging times analyzed were 3, 6, and 12 months. Four-point bending was likewise utilized to assess the flexural modulus and load at failure.

As in the prior chapter, uncoated ACCC rods were received from the Western Area Power Administration (WAPA) from an unused full conductor reel. These samples arrived in 5 foot sections. The hybrid composite cores have an outer diameter of 9.53 mm with the carbon section having a diameter of roughly 6.8 mm. Some of the hybrid cores were sent to E.L. Stone Company who applied a proprietary fluorinated ethylene propylene (FEP) based coating with a thickness of approximately 25 microns. The rods were lightly sandblasted prior to the application of the coating to improve adhesion. As noted previously no evidence of surface damage was visible even under 100x optical imaging (see Figure 2-2).

Coated and uncoated rods were cut to lengths of 28 cm. The ends of each rod were capped with an RTV sealant to prevent longitudinal oxidation from the ends. Samples were aged at 200 °C under atmospheric conditions. Three samples of coated and uncoated rods for each aging duration were produced and tested. Samples were heated and cooled at a rate of 5 °C per minute to reduce the risk of thermal shock.

Samples were tested in a four-point bend test fixture designed by Burks et al [4]. As suggested in [4], samples were loosely wrapped with Teflon tape at the contact point with the loading pins to prevent transverse crushing. The load rate was 3 mm/ minute. Center point displacement measures, using an LVDT, and force measures were taken at a 20 Hz sampling rate. Crosshead displacement continued until failure of the samples.

3.3 Results

Figure 2-1 shows as received ACC core rods before and after coating. Figure 3-1 shows the rods after 12 months of aging at 200 °C.

Figure 3-1. Aged ACCC core samples. As received (top) and coated (bottom).

As in the prior chapter, all samples aged at 200 °C failed in shear in the horizontal midplane of the rods in the four-point bend test. Table 3-1 shows the average load at failure and flexural modulus of the three samples tested for each aging duration.

Table 3-1. Load at failure and flexural modulus of aged samples

Load at failure (N)	Unaged	3 Month	6 Month	12 Month
200 °C Coated	4598	2357	2067	1847
200 °C Uncoated	4616	2959	2364	1987

Flexural Modulus (MPa)	Unaged	3 Month	6 Month	12 Month
200 °C Coated	82.5	79.9	80.3	79.6
200 °C Uncoated	80.9	80.4	81.7	81.6

3.4 Comparison to 180 °C

As noted in Table 3-1 core rods aged at 200 °C lose flexural strength with increased aging times, but generally maintain or improve their stiffness. It is believed that stiffness increases with post-curing (the rods are manufactured with a rapid curing cycle

in a pultrusion process) and from the effects of physical aging. However, physical aging also increases the residual stresses in the rods as demonstrated by Middleton et al [6]. As aging time increases, so do the residual stresses leading to a lower flexure load at failure. Thus, we see a steady drop in the flexure load at failure.

The situation becomes more interesting as a comparison is made to the results of aging at 180 °C from the prior chapter. Figure 3-2 shows the flexure loads at failure for the samples aged at 180 °C and 200 °C. From this figure, it can be seen that initially the loads at failure drop faster for 200 °C aging than for 180 °C. Also, in both cases the load at failure continues to steadily decline as aging time increases through the first six months (and in fact 9 months for rods aged at 180 °C, as noted in the prior chapter- see Figure 2-9).

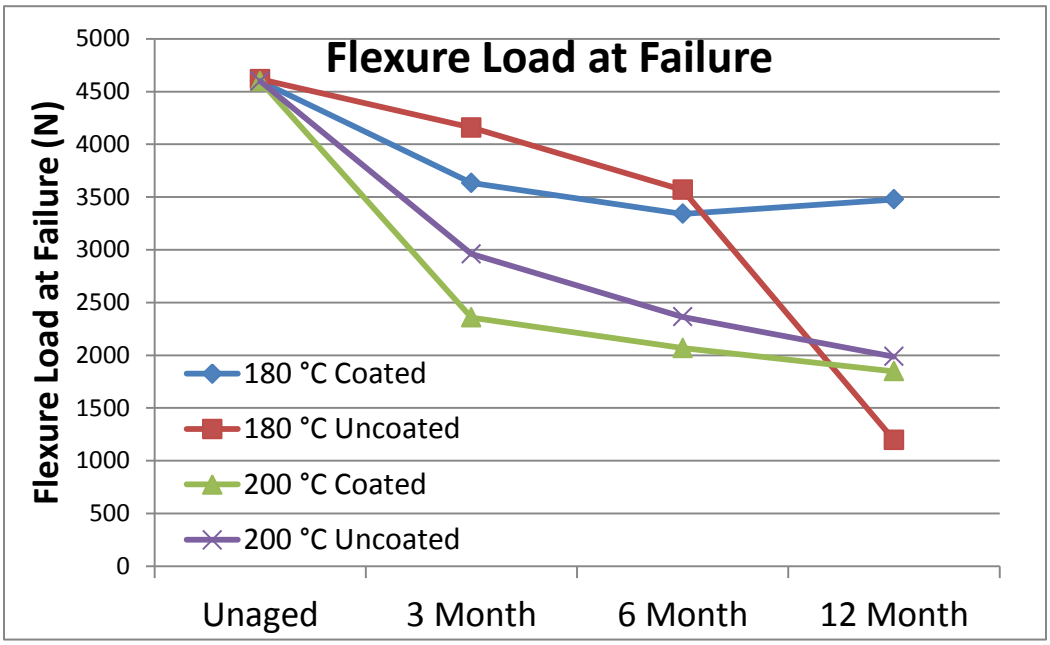

Figure 3-2. Flexural load at failure for ACCC rods after specified aging time and temperature.

However, at 12 months, the uncoated rods aged at 180 °C show a dramatic dropoff in the load at failure, a reduction that is not seen in the coated rods aged at 180 °C or in the coated or uncoated rods aged at 200 °C. It is believed that this steep dropoff for the 180 °C uncoated rods is due to thermal oxidation of the surface of the rods producing

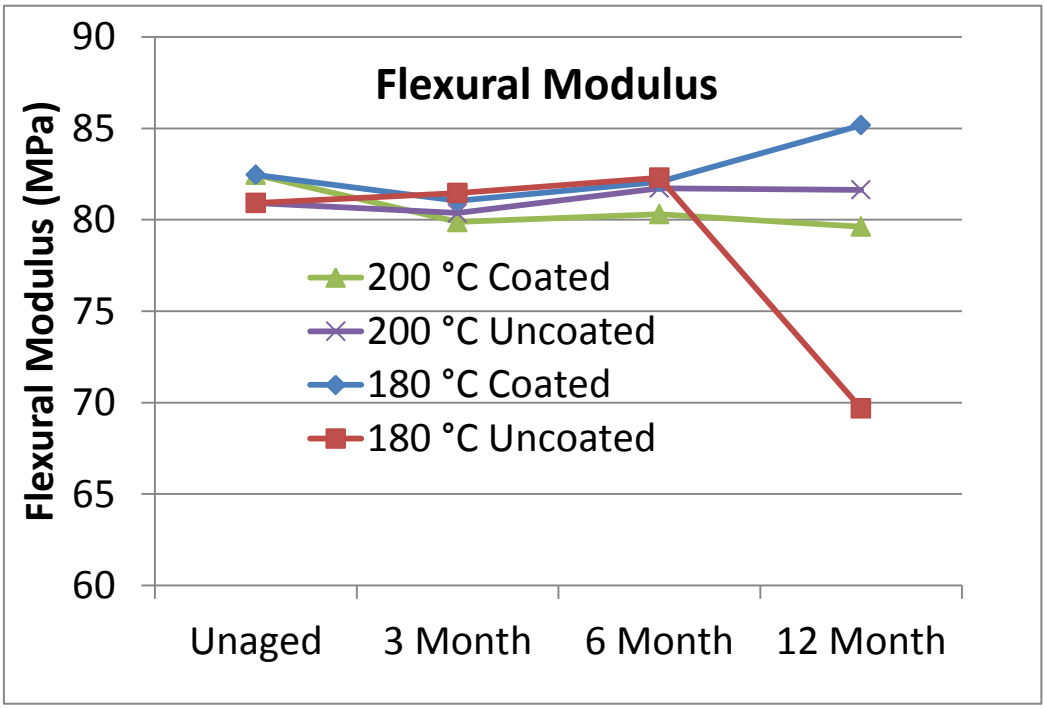

Figure 3-3: Flexural modulus for ACCC rods after specified aging time and temperature.

cracks large enough to create stress concentrations that can be the initiation point for shear failures. This chemical aging might not occur on the coated rods aged at 180 °C because the coating acts as an oxidation barrier. Thus, as opposed to aging at 180 °C we do not see this same dramatic dropoff in the flexure load at failure. Figure 3-3 shows a comparison of the changes in flexural modulus for the four aging temperature/coating conditions. Here again there is a dramatic dropoff for the 180 °C 12 month aged rods and

again it is believed that chemical aging is responsible for destroying enough of the surface matrix to reduce the stiffness of the whole material.

So, why is there not this same dropoff for uncoated rods aged at 200 °C? Barjasteh et al [3] performed oxidation experiments on the core rods and modeled the oxidation reaction in the epoxy at both 180 °C and 200 °C. What they found was that the depth of oxygen penetration was actually lower at the higher temperature of 200 °C than it was for 180 °C. From visual inspection of aged samples they found the oxidation thickness was 155 μm for aging at 180 °C but only 110 μm for aging at 200 °C. This surprising result was reinforced by their numerical model of the oxidation reaction. The Barjasteh model was reproduced and its results are displayed in Figure 3-4 where the oxygen concentration is displayed as a function of the depth below the surface after 100 hours of aging. There is negligible change in the modeled oxygen concentration beyond 100 hours at either temperature.

Basically, thermal oxidation occurs through a reaction diffusion mechanism. While both the diffusion rate and the reaction rate of oxygen with the epoxy polymer (consumption rate) escalate with increasing temperature, the consumption increases at a faster rate than the diffusion so the oxygen does not penetrate as far into the bulk of the polymer, unless as Barjasteh et al [3] points out there is significant cracking or surface erosion which would allow deeper oxygen penetration.

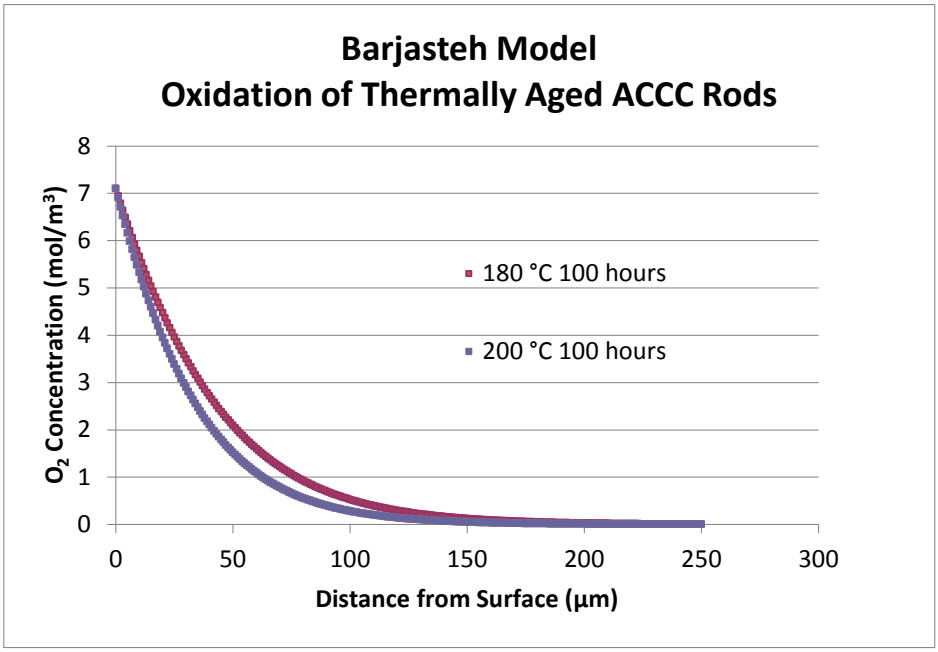

Figure 3-4. Oxygen concentration as a function of distance from the surface.

Thus, it is believed the deeper oxygen penetration at the lesser 180 °C temperature eventually creates cascading damage on the surface leading to a dramatic drop in flexural stiffness. The cracks on the surface also create an initiation point for shear failure which reduces the flexural load at failure. Less chemical aging occurs at the higher 200 °C temperature and these same dramatic effects are not observed.

3.5 Summary of Chapter 3

Below the glass transition temperature, higher temperatures lead to more rapid physical aging and increased residual stresses in the bulk of the material. Applying a coating to the hybrid rods does not affect its physical aging. This physical aging has a small impact on the stiffness of the rods, but a larger impact on the flexure load at failure. Thus a higher aging temperature reduced the flexure load at failure at early aging durations for both coated and uncoated rods.

However, the chemical aging involves a diffusion-reaction mechanism. While higher temperatures lead to a more rapid diffusion of oxygen, the oxygen polymer (epoxy) reaction rate increases even faster with a higher temperature (200 °C vs. 180 °C). Thus the oxidation thickness actually decreases with increasing aging temperature. Therefore, at the higher 200 °C aging temperature, there was not a shift in the source of flexural failure from physical aging to chemical aging and thus there was no dramatic dropoff in the flexure load at failure for aging durations through twelve months. This result reinforces the hypothesis that chemical aging led to the dramatic dropoff in flexure load at failure for the uncoated rods aged at 180 °C.

CHAPTER 4 EMISSIVITY EFFECT ON OPERATING TEMPERATURE

4.1 Introduction

Another way of reducing thermal aging in polymer core composite conductors is to reduce the amount of heat to which the conductor core is exposed. Reducing the current flowing in the conductor is one obvious way to lower the temperature and diminish the thermal aging. However, this approach reduces the value of this HTLS conductor to the transmission companies. Wind speed can also significantly reduce the operating temperature of transmission lines [15, 16, 17] through convective cooling. However, on very calm days, this reduction does not happen.

An innovative approach to reducing operating temperature is to increase the radiative cooling from the conductor. Companies are developing coatings to be applied to the outside surface of the aluminum conductor itself to increase the emissivity. Increasing the emissivity increases the radiative cooling and can therefore allow the conductor to transmit the same current while maintaining a lower temperature.

4.2 Methods

An experimental and a modeling approach were used to determine the value of increasing the emissivity of the conductor. In the experimental approach, two samples of an ACCC conductor were heated in an oven to a temperature slightly above 80 °C. One of the samples was as received and the other was painted black in order to increase its

emissivity. Note that this black painting was simply a method to test the impact of changes in emissivity and not any commercially developed coating. The as received conductor was actually from a sample reel that had been exposed to elements in Phoenix, Arizona for about ten years and as such would represent a conductor with emissivity closer to that which might be found in-service rather than a brand new conductor. No attempt was made to eliminate heat loss from the ends of the conductors in this rudimentary test.

A thermocouple was inserted into the end of each sample and a Lascar datalogger was used to record the temperature at 1 second intervals. Both samples were allowed to cool to 80 °C before the measurement period was begun in order to have a fair comparison of cooling rates. Both samples were cooled in an atmospheric environment with a temperature of 20 °C.

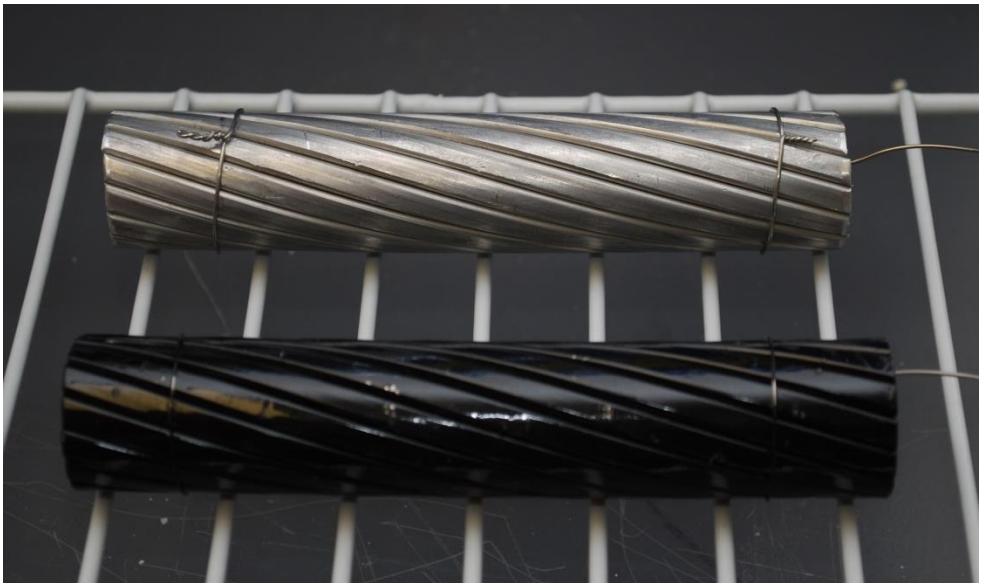

Figure 4-1. Shiny (as received) and black painted ACCC conductors.

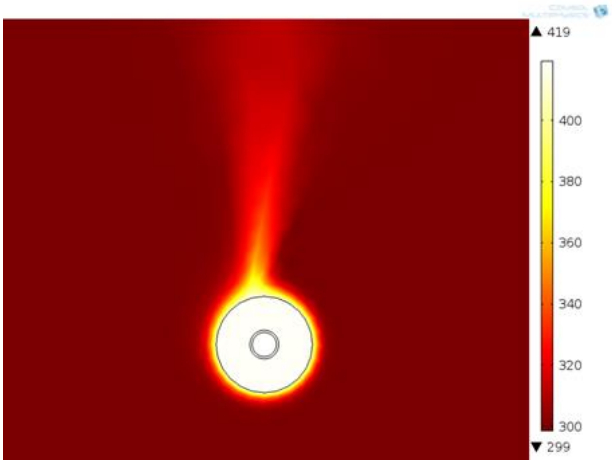

Figure 4-2. Early heating of the whole conductor with no wind

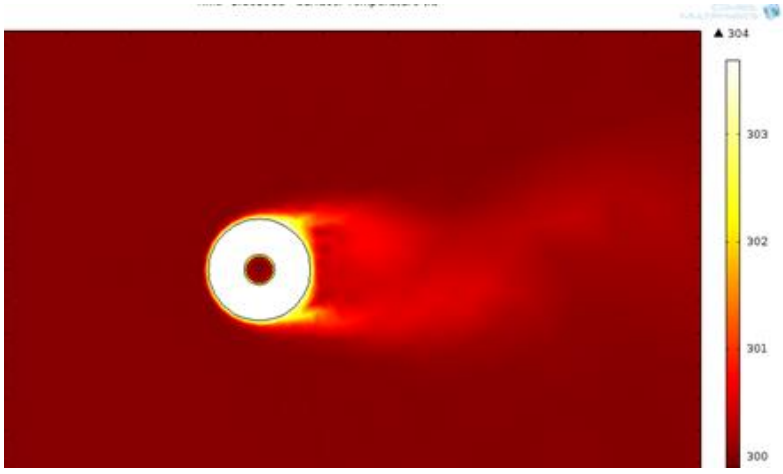

Figure 4-3. Early heating of the conductor with wind

A finite elements model of the conductor was built to model the impact of wind speed and emissivity on the temperature of the conductor given a fixed amount of resistive heating. For this 2 dimensional simulation, the radius of the carbon fiber epoxy composite portion of the rod was set at 4.0 mm, the glass fiber epoxy radius was set at 4.8 mm, and the aluminum conductor radius was set at 15.9 mm. These components were modeled as concentric circles, so helical stranding was not considered. The air domain was 400.0 mm wide and 200 mm high and the center of conductor was positioned one

fourth of way over from the left and one fourth of the way up in this 2d "box" to allow for convection in the opposite directions from gravity and simulated wind. The gravimetric force was set at 9.8 m/s^2 and laminar flow was utilized with the inlet on the left and no pressure on the right hand boundary. The starting temperature for all domains and ambient air temperature were set to 300 K and the pressure was set at 1 atmosphere. The volume force for the air was determined as –(353.0563/T – 353.0563/300) * G, where T is the temperature and G is the gravimetric force. The density, thermal conductivity, and heat capacity are indicated in Table 4-1.

Table 4-1. Density, thermal conductivity, and heat capacity of epoxy carbon fiber composite (CFC), epoxy glass fiber composite (GFC), aluminum and air.

Material	Density (kg/m^3)	Thermal Conductivity (W/(m*K))	Heat Capacity (J/(kg*K))
CFC	1043	0.17	800
GFC	1168	0.2	1000
Aluminum	2700	238	900
Air	0.02897/8.314/T	0.00227583562 +1.15480022E-4*T^1 -7.90252856E-8*T^2 +4.11702505E-11*T^3 -7.43864331E-15*T^4	1047.63657- 0.372589265*T^1 +9.45304214E-4*T^2 -6.02409443E-7*T^3 +1.2858961E-10*T^4

The power of this thermal heating was set at 0.19 $watts/cm^3$ such that with no wind and no radiative cooling, the temperature of the conductor would asymptotically approach 180 °C. The simulated heating was applied for 5000 seconds followed by a cooling period of 1000 seconds. This simulation was conducted under various wind speeds and emissivity values, using the same resistive heating power level. Figure 4-2 shows a temperature graph of the cross section of the entire conductor and the

surrounding atmosphere early on in the heating process, indicating convective heat losses moving away from the conductor fastest in the up (anti-gravity) direction. Figure 4-3 shows the same conductor being heated with the same energy, but with a constant cross wind. Note forced convective heat losses being carried by the wind.

4.3 Results and Discussion

Figure 4-4 shows the result of the measured cooling rates of the as received

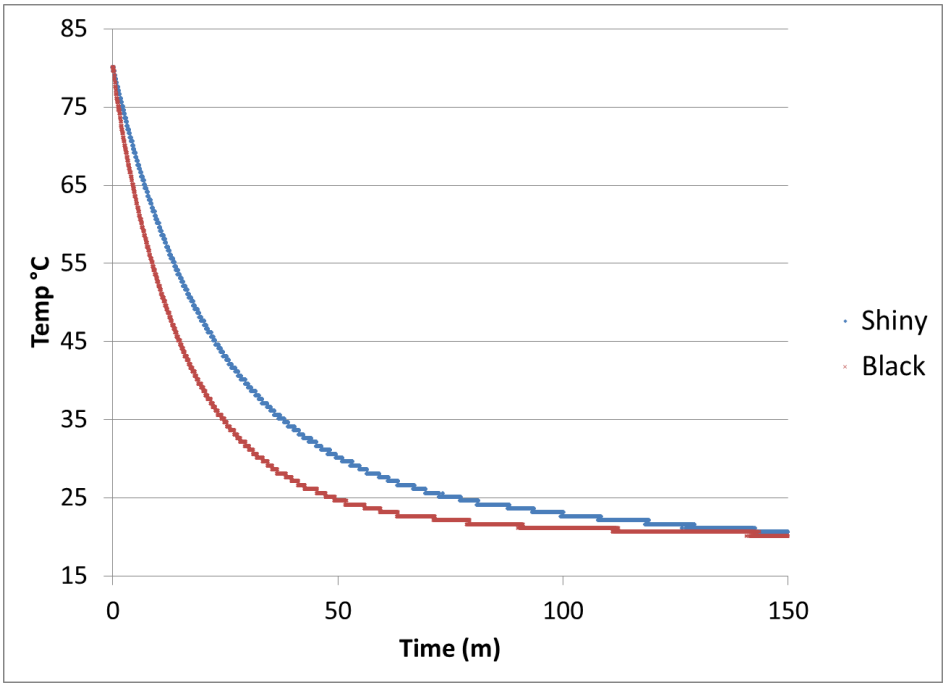

Figure 4-4. Internal temperature comparison between shiny (as received) and black ACCC conductors cooling in air at room temperature

(shiny) conductor and the painted black conductor. Initially, the painted black conductor cooled at a rate nearly twice that of the as received conductor. These cooling rates included both radiative and free convective cooling. Thus, as expected, there was a significant increase in the cooling rate of the painted black conductor due to the

emissivity increase. Radiative cooling increases with the fourth power of the temperature, so the difference would be considerably greater as temperatures approach 180 °C rather than 80 °C.

In the finite elements model, there was a significant difference in the equilibrium

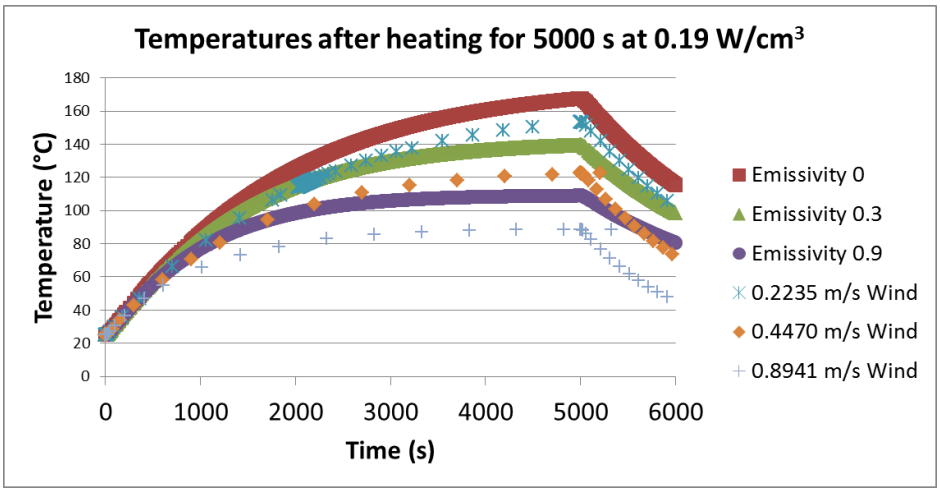

Figure 4-5. Temperature under heating and cooling for various wind and emissivity conditions

temperature of the conductor given different wind and emissivity conditions. Figure 4-5 shows that the temperature of the conductor with no wind and no radiative cooling approaches an equilibrium temperature of 180 °C when heated at 0.19 watts/cm^3. However, when radiative cooling is considered with an emissivity value of 0.3, the equilibrium temperature approaches about 145 °C, or about 35 °C less. With an emissivity of 0.9, there is enough radiative cooling to bring the equilibrium temperature down to about 115 °C.

Wind can also make a significant difference in the equilibrium temperature of the conductor. A constant transverse wind speed of only 0.224 m/s (0.806 km/h) on a 0 emissivity conductor produces a very similar heating and cooling pattern as the 0.3

emissivity simulation. Likewise, doubling the wind speed to 0.447 m/s (1.61 km/h) produces a heating/cooling pattern that is very close to the 0.9 emissivity model. While these may be low wind speeds, as pointed out in [15] the angle of the wind can have a significant impact on the convective cooling. Hot calm days may also increase electricity demand in the United States as air conditioning usage increases [18].

4.4 Summary of Chapter 4

A surface coating that provides an emissivity increase can potentially reduce the operating temperature of a conductor. For this approach to be effective and beneficial, the coating must increase the emissivity to hasten radiative cooling; however, the coating must be carefully designed so that the emissivity increase does not also increase radiative absorption from the sun. This selective tuning can be accomplished by selecting materials that emit and absorb higher at specific wavelengths in order to increase the emissivity in the infrared range but reduce it in the wavelength range of sunlight. Thus, a surface coating to increase emissivity for certain wavelengths can be one element in the protection against thermal aging.

CHAPTER 5 RESEARCH ON EPOXY NANOCOMPOSITES

5.1 Introduction

5.1.1 Overview

Nanoparticles added to epoxies can dramatically change the thermoset's thermal and mechanical properties. Trying to identify the optimal nanoparticle to tune specific properties is a challenging task. There is a large and growing population of studies that look at incorporating different types of nanoparticles into various epoxy systems to see the impact on the glass transition temperature (T_g), strength, stiffness, toughness, and other mechanical properties. The effects not only depend on the type of nanoparticle, but also its size, dispersion, and functionalization, as well as the amount (concentration) of the nanoparticle added. In some cases there is a monotonic material property response, but in others an optimal concentration can be identified.

5.1.2 Background

For years researchers have been searching for ways of improving the thermal and mechanical performance of polymers. Fillers have been used to improve toughness, stiffness and resistance to oxidation. Recently, researchers have turned to a new type of filler: nanoparticles. Nanoparticles are often described as particles with at least one

dimension less than 100 nanometers (100 x 10^{-9} meters). Because of their large surface to volume ratio, nanoparticles of a material can have significantly different properties from larger bulk portions of the same material.

There are a significant number of epoxy resins, hardeners, and nanoparticles. To make a useful epoxy thermoset, there must be at least one epoxy and one hardener. There are published books on the properties of various combinations of epoxies and curing agents (see, for example, 'Handbook of Epoxy Resins' [19]). One possibility to improve the long-term performance of the epoxies in the new electrical conductors is to incorporate nanoparticles into the epoxy matrix to protect against thermal damage. There have been a large number of studies looking at the impact of various nanoparticles on mechanical, thermal and electrical properties of epoxies. Common nanoparticles added to epoxies to modify properties include silica (SiO_2), alumina (Al_2O_3), graphene, carbon nanotubes, nanoclays, and carbon black. As will be seen, it is not enough to simply specify the nanoparticle and the epoxy/ resin combination; different concentrations of nanoparticles can create significantly different properties. The property changes are usually non-monotonic, with optimal concentrations only determined by experiments. Different sized nanoparticles can also be utilized, creating different properties. Within each class of nanoparticles, there are various properties of the nanoparticles themselves such as porous and non-porous silica, multiwalled and single walled carbon nanotubes, and highly conductive and not as highly conductive carbon black. Of course, one can also use a combination of nanoparticles to create even more possible nanocomposites, as well as changing the approach to dispersion or functionalizing (adding functional groups or

coatings to the surface of the nanoparticles) in order to achieve different results. Thus, there are an infinite number of possibilities. In order to help select appropriate nanoparticles to enhance the material properties of the epoxies utilized in high voltage applications, this chapter summarizes the recent published experiments with silica, carbon black, graphene, nanoclay, carbon nanotubes, and alumina nanoparticles.

5.2 Epoxy Nanocomposites

5.2.1 Silica

There are many types of silica (SiO_2) nanoparticles [20,21]. The silicon atom forms a tetrahedral bonding structure with its neighboring oxygen atoms. While quartz is a well-known crystalline silica structure, most of the nanoparticles utilized in polymer nanocomposite studies are amorphous forms of silica, i.e., there is no long range regular crystal structure. Within the amorphous class of silica particles, there are many different forms. One classification is the porosity of the particles: P identifies porous structures, those with large pores; N identifies nonporous structures, particles with very small pores. Nonporous structures are denser than porous structures. Mesoporous silica falls in the middle, with medium size pores (2-50 nm). The structure of the surface and whether or not there are hydroxyl (OH) groups present, determines the hydrophobicity or hydrophilicity of the nanoparticle. Silica is electrically non-conductive. Most of the nanoparticles that are reviewed in the following studies are in the size range of 7-30 nm with a couple of studies looking at larger nanoparticles.

Zhang et al [22] conducted experiments adding various concentrations (0-22.7 wt %) of 25 nm silica nanoparticles to a cycloaliphatic epoxy with an anhydride hardener.

They found that the flexural modulus increased with increasing silica content, improving from 3.05 GPa for the neat epoxy to 4.18 GPa for the epoxy with 22.7% silica. For small concentrations of silica, the flexural strength was diminished by about 7%; for larger concentrations in excess of 10 wt%, there was a small improvement. The strain at failure was reduced for all concentrations of silica, but was not monotonic with silica content. Both the microhardness and toughness showed improvements with increasing silica content. The glass transition temperature (T_g) generally decreased with increasing silica content, moving from 222 °C for the neat epoxy to 208 °C for 22.7% silica.

Ou et al [23] worked with different sized silica nanoparticles at different concentrations to determine the impact on glass transition temperature (measured by DSC) and water permeability. This group used three different sized nanoparticles, 20, 12, and 7 nm, and varied the concentration from 0.3 wt% to 7 wt% in a DGEBF epoxy hardened by m-phenylenediamine. There was an immediate increase in the glass transition temperature, moving from 63 °C (for the neat epoxy system) to 72 °C for the 0.3 wt% concentration of 20 nm silica and to 83 °C for the same concentration of 7 nm nanoparticles. In general, the glass transition temperature continued to improve as the concentration of nanosilica was increased, with 7 wt% 20 nm particles reaching 79 °C and 7 wt% 7 nm particles reaching 98.2 °C, an overall increase of 35 °C. The authors attributed the T_g increase to good adhesion between the nanoparticles and the matrix and the ability of the nanoparticles to restrict segmental motion of the polymer. The authors also found that silica nanoparticles would reduce water permeability of the epoxy. Again, the best improvements were found for the 7 wt% 7 nm silica nanoparticles, reducing the

water permeability by 30%. The same concentration of 20nm silica reduced the water permeability by only 10%. Thus the authors found that the impact of silica nanoparticles was influenced both by the size and the concentration of the particles.

Allahverdia et al [24] also conducted experiments with nanosilica and epoxy, utilizing bisphenol A and epichlorohydrin hardened by a cycloaliphatic amine. The nanosilica particles were 10 nm in size and were used in concentrations of 1, 3, and 5 wt%. In these experiments, a small increase in T_g of about 5 °C was found for the 3 wt% nanocomposites (an increase from 48.9 °C to 54.2 °C, as found by DMA), with slightly lesser improvements for the other concentrations. Both the nanohardness and elastic modulus increased with increasing silica content, increasing more than 20% each for the 5 wt% nanocomposites.

Tzetzis et al [25] performed nanoindentation and tensile tests on epoxy with fumed silica nanoparticles. The epoxy was bisphenol A and epichlorohydrin epoxy resin (Epikote 816) with an amine curing agent. The nanoparticles were untreated fused silica with an average particle size of 20 nm. They performed tests on samples with 0.5, 1, 2, and 3 wt% silica and found that the elastic modulus calculated by both the tensile test and the nanoindentation method was reduced with increasing silica content. The modulus was reduced by about 25% for the 3 wt% sample. They attributed the reduction to the formation of agglomerates of silica, in which the modulus was less than in the epoxy. Thus poor dispersion could have been the problem leading to the reduction in modulus.

On the other hand, Conradia et al [26] found improved mechanical properties upon including silica nanoparticles in an epoxy composed of bisphenol A and

epichlorohydrin (Epikote 828LVEL) with 1,2-Diaminocyclohexane as the hardener. In these experiments, two different sizes of nanoparticles, 30 nm and 130 nm, were first treated with diglycidyl ether of bisphenol A (DGEBA) and then added to the epoxy at a concentration of 0.5 vol% in order to compare the impact of the size of the nanoparticles. For both sizes of nanoparticles, the tensile modulus, the tensile strength, and the fracture toughness of the nanocomposites were improved compared to the neat epoxy. In general, the 130 nm nanosilica created the better improvement, with the tensile modulus increasing about 15%, the tensile strength improving about 11%, and the fracture toughness improving about 38%. The corresponding improvements for the 30 nm nanosilica were 8%, 11%, and 41%.

Dittanet and Pearson [27] studied the impact of different sized organosilane coated silica nanoparticles on DGEBA cured with piperidine. They used 23, 74, and 170 nm nanoparticles with volume concentrations ranging from 2.5 to 30% for each sized particle. They found that the T_g varied with particle size and concentration, but that it generally remained within ± 2 °C from the value for the neat epoxy, not a very significant change. Similar to T_g, the yield strength also varied about the reported value for the neat epoxy, with the results generally within 2% of the value for the neat epoxy. On the other hand, the authors found a significant stiffening of the nanocomposites which increased with nanoparticle concentration. The largest increase in the Young's Modulus was for the 30 vol% 170 nm silica nanoparticles, increasing the stiffness by 65%. The coefficient of thermal expansion (CTE) was also improved (reduced) with increasing particle content, but this time the largest reductions came with the smallest (23 nm) particles. Small

reductions of about 7% were found for the 2.5 vol% samples, but the CTE for 30 vol% 23 nm silica was reduced by 54%. Fracture toughness also improved significantly with all of the tested concentrations, but showed further large increases as the concentration was increased. For example, for the best performing 74 nm particles, the fracture toughness increased 58% for the 2.5 vol% samples and 160% for the 30 vol% samples.

Sajjad et al [28] looked at the impact of 9 and 74 nm silica nanoparticles, surface functionalized with diethyleneglycol-based capping agents, on a DGEBF epoxy cured with diethylenetriamine (DETA). This study evaluated the impact on T_g, storage modulus, and hardness for volume concentrations of 1.7, 2.9, and 5.8%. The authors also used two different sized nanoparticles, 9 nm and 74 nm, in order to see if there was also an impact due to size. The authors found that adding and increasing the concentration of nanoparticles reduced the T_g and even more significantly reduced it for the larger nanoparticles. At the 1.7 vol% concentration of 9nm nanoparticles, the T_g was reduced by about 7 °C; for the 74 nm nanosilica at 5.8 vol%, the T_g was reduced by about 30 °C. The storage modulus at room temperature, however, improved with increasing nanoparticle content, with the best increase (about 25%) occurring for the larger particles at the highest concentration of 5.8%. Similarly, the hardness measured by the Vickers hardness test increased 40% for the larger nanoparticles at the highest concentration with much lesser improvements for the smaller nanoparticles (only 10% improvement for the highest concentration).

Johnsen et al [29] looked at the impact of organosilane coated 20 nm silica on DGEBA epoxy cured with methyl-hexahydrophthalic acid anhydride (MHHPA). They

measured the T_g using both DMTA and DSC and found little or no change even with weight concentrations up to 20.2%. However, they found an increase in both stiffness and fracture toughness with increasing silica content. For the Young's Modulus, they found a 30% increase with a silica content of 13.4 vol%. For fracture toughness, the G_{1c} value increased by 140% for the same 13.4 vol%. There were lesser, but still significant, improvements in both of these material properties for lower vol% of nanosilica. In this paper, they also discussed the mechanisms for the significant increase in fracture toughness. They propose that the main factor leading to increased toughness is debonding of the particles followed by plastic void growth. Due to the size of the particles being much smaller than the calculated crack tip opening displacement, they discount the contribution from crack pinning. Similarly, because the roughness of the fracture surface does not correspond to the increased fracture toughness, they rule out crack deflection as a significant factor in the improvement in G_{1c}.

In a study with very similar materials, Hsieh et al [30] evaluated the impact of silica nanoparticles on a DGEBA epoxy with a methylhexahydrophthalic acid anhydride hardener. They looked at T_g, tensile modulus, and fracture toughness. For T_g, they found little change with the addition of the nanoparticles, but found increasing stiffness and fracture toughness with increasing wt% of silica. For 4 wt% silica, the stiffness increased by about 8%, while for 20 wt% the stiffness improved by 30%. Similarly, fracture toughness increased by about 25% for the 4 wt% silica and by about 72% for the 20 wt % silica.

Zheng et al [31] first examined the impact of uncoated 20 nm silica nanoparticles on the glass transition temperature and the thermal mechanical properties of an MHHPA cured cycloaliphatic epoxy. The impact on the glass transition temperature varied depending on the method used: using DSC, they found a small decrease in T_g for 1, 2, and 3 wt%, but a large decrease of 11 °C for 5 wt%; using DMA, there was a small decrease for 1 and 2 wt%, but a small increase for 3 and 5 wt%. They also found that flexural strength increased with increasing silica content, as much as a 19% improvement for 5 wt%. On the other hand, they found that the impact strength as measured by a Charpy test was highest for 3 wt%, with a falloff in strength for 5 wt%. The 3 wt% nanocomposites improved the impact strength by 24%. In a follow-up study, Huang and Zheng [32] explored the impact of surface treatment on the electrical resistivity and dielectric breakdown strength of the cycloaliphatic epoxy silica nanocomposites. Since, as they noted, cycloaliphatic epoxies are often used as an insulative material in electrical applications, they sought to understand whether surface treating the nanosilica could improve its electrical properties. They found that incorporating (3-Glycidoxypropyl) methyldiethoxysilane (GPMDS) as the silane coupling agent improved both the resistivity and dielectric breakdown strength, especially at higher temperatures.

Ragosta et al [33] explored the impact of 10-15 nm nanosilica on the glass transition temperature and fracture toughness of TGDDM epoxy cured with diaminodiphenylsulfone (DDS). They found a small decrease in T_g of about 7 °C at both 5 and 10 wt% from the neat epoxy value of approximately 240 °C. They attributed this loss to unreacted epoxide groups in the presence of the nanoparticles. In spite of the lack

of a complete reaction, they found a significant improvement in the elastic modulus and yield strength. These enhancements showed nearly linear increases with increasing wt% of silica. At 10 wt%, the improvement was about 50% for stiffness and 28% for strength. Similarly, they found a large increase with increasing silica content in both the critical stress intensity factor K_c and the strain energy release rate G_c. K_c approximately doubled and G_c approximately tripled at 10 wt% silica.

In summary, nanosilica can have impacts on thermal and mechanical properties. The effect on the glass transition temperature is inconsistent; some studies show improvements, others little impact, and still others show a reduction. However, concentrations of nanosilica can be optimized to achieve improvements in elastic modulus and toughness. Dispersion is important and functionalization of nanosilica especially with silane containing molecules can bring about more significant improvements. Electrical properties can also be improved by the incorporation of nanosilica.

Table 5-1. Silica Nanocomposites

Author (Year)	Nanoparticle(s)	Concentrations	Epoxy System	T_g	Stiffness	Strength	Toughness	Other
Zhang (2006)	Silica - 25 nm	1.8, 5.3, 10.3, 16.7, 19.7, and 22.74 wt%	Cycloaliphatic/Anhydride	Generally decreasing with increasing silica content, moving from 222 °C to 208 °C for 22.7 wt% silica	Increasing with increased silica content up to 28% increase at 22.7 wt%0. Flexural stiffness increased with increased silica content up to 37% increase at 22.7 wt%	Flexural strength showed small increases for large wt% but small decreases for low wt%	Increasing with increased silica content up to 76% in K_{1c} and 148% in G_{1c} increase at 22.7 wt%	
Ou (2008)	Silica 20, 12, and 7 nm	0.3, 0.5, 1, 3, 5, and 7 wt%	DGEBF/m-phenylenediamine	Significant Increases at low and high wt% (0.3 - 7 wt%). Best was 35 °C increase to 98 °C at 7 wt% 7 nm nanosilica				Water Permeability decreased with increasing silica, best was 30% reduction for 7 wt% 7 nm silica
Allahverdia (2012)	Silica 10nm	1, 3, and 5 wt%	DGEBA/cycloaliphatic amine	Small improvements in T_g. 3 wt% was optimal (better than 1 & 5 wt%) showing an increase of 5 °C				nanohardness increased with increasing silica content up to % at 5 wt%
Tzetzis (2013)	fumed silica 20nm	0.5, 1, 2, and 3, wt%	DGEBA/amine		Reduction in stiffness with increasing silica content up to 25% reduction at 3 wt%			
Conradi (2013)	silica 30 and 130 nm	0.5 wt%	DGEBA/1,2 Diaminocyclohexane			Improvement of 11% and 11% for the 130 nm and 30 nm nanosilica	Improvement of 38% and 41% for the 130 nm and 30 nm nanosilica	
Dittanet (2012)	organosilane coated silica 23, 74, and 170 nm	0, 2.5, 5, 10, 15, 20, 25, and 30 vol%	DGEBA/piperidine	Small changes (< 4 °C) that varied depending on particle size and concentration		Insignificant changes up and down depending on particle size and concntration	Significant increases in K_{1c} and G_{1c} for all particle sizes and concentrations. Best was 160% improvement in K_{1c} and 317% improvement in G_{1c} for 30 vol% 74 nm nanosilica	Coefficient of Themal Expansion (CTE) was reduced with increasing silica content up to a 37% reduction at 30 vol%
Sajjad (2011)	diethylene glycol coated silica 9 and 74 nm	1.7, 2.9, and 5.8 vol%	DGEBF/DETA	T_g reduced with increasing concentration and particle size up to about 30 °C for 5.8 vol% 74 nm silica				vickers hardness improved with increasing concentration. The larger nanoparticles had a much more significant impact with the 5.8 vol% 74 nm nanocomposite showing an increase of 40%
Hsieh (2010)	surface coated (unspecified) silica 20 nm (Nanopox F 400)	0, 4, 7.8, 11, 15, and 20 wt%	DGEBA/methylhexahydrophthalic acid anhydride (MHHPA)	Insignificant changes			Increasing with increased silica content up to 72% increase at 20 wt%	
Johnsen (2007)	organosilane coated silica 20 nm	0, 4.1, 7.8, 11.1, 14.8, and 20.2 wt %	DGEBA/MHHPA	Insignificant changes			Increasing with increased silica content up to 141% increase at 20.2 wt%	
Zheng (2008)	silica 20 nm	0, 1, 2,3, and 5 wt%	Cycloaliphatic/MHHPA	Decrease using DSC with a large decrease at 5%; Using DMA, small decrease for 1 & 2 wt%, small increase for 3 & 5 wt%		Flexural strength Increased with increased silica content up to 19% increase at 5 wt%		Charpy impact test: Improvement of 24% for 3 wt%, but a reduction for 5 wt%
Ragosta (2005)	Silica 10-15 nm	0, 3, 5, 7, and 10 wt%	TGDDM/DDS	Decrease of about 7 °C for both concentrations		Increasing with increased silica content up to 28% increase at 10 wt%	Increasing with increased silica content: K_c increased ~100% and G_c ~200% for 10 wt%	

5.2.2 Carbon Black

Carbon black is a paracrystalline form of carbon, formed from the incomplete combustion of petroleum products [34]. Its primary particle size can be as small as 20 nm, but agglomerates tend to form creating larger amorphous structures. It is generally a conductive material, but its conductivity can be tuned. Historically, it has been used as a reinforcing agent in tires to increase wear resistance.

Kosmidou et al [35] tested thermal and mechanical properties of various concentrations of carbon black with a DGEBA epoxy cured with triethylenetetramine (TETA). The carbon black was described as highly conductive and had particle sizes of 25-75nm. The researchers varied the carbon black weight percentage from 0.05% to 2.0% and found dramatic changes in T_g. Small increases in T_g were noted for concentrations of 0.05 and 0.1%, but for a concentration of 0.5%, a dramatic increase of 37 °C was found. For higher concentrations, the T_g was still significantly increased but was less than for the 0.5% concentration. For example, the 2.0% concentration had only a 13 °C increase in T_g. They also found small improvements in the storage modulus with the addition of carbon black, but the optimal concentration depended on testing temperature.

Ma et al [36] explored the addition of D-220 carbon black (24-33 nm particle size) to a Bisphenol-A epichlorohydrin epoxy cured with Methyl-tetrahydrophalic anhydride (MeTHPA). In their experiments they used different concentrations (1-5 wt%) of carbon black coated with a silane coupling agent. They found significant improvements in tensile strength, elongation at break, and flexural strength, with the greatest increase coming from a 2.0 wt% loading of carbon black. With the 2% loading,

the tensile strength increased 32% and the flexural strength increased by 89%, while the elongation at break increased by 40%. Smaller improvements were found for lower and higher concentrations of carbon black. They also found an increase in T_g at 2 wt% and an even larger increase at 5 wt%.

Kim et al [37] explored the impact of 35nm carbon black (Ketjenblack EC-300J) of various concentrations on the fracture toughness of bisphenol-A epoxy cured with polyetheramine. At room temperature, they found a significant increase of 18% and 23% in K_{1c} for the 2 wt% and 3 wt% concentrations respectively. Smaller increases were found for lesser concentrations.

While there are not a large number of studies evaluating the impact of carbon black on thermal and mechanical properties of epoxies, there seems to be the potential for significant improvement in the glass transition temperature, strength and toughness. Electrical resistivity drops after reaching the percolation threshold, so for certain applications care will need to be taken to avoid this situation.

Table 5-2. Carbon Black Nanocomposites

Author (Year)	Nanoparticle(s)	Concentrations	Epoxy System	T_g	Stiffness	Strength	Toughness	Other
Kosmidou (2008)	extra conductive carbon black (25-75 nm)	0, 0.05, 0.1, 0.5, 0.7, 1, 2 wt%	DGEBA/TETA	Significant improvement in T_g at 0.5 wt% (37°C); small improvements below that concentration and large but not quite as great improvements above that concentration.				Electrical resistivity showed little change until concentration level reached 1.0 wt%. At 1.0 % and above, the resitivity showed a significant (and growing) reduction.
Ma (2010)	silane modified carbon black N220 (24-33 nm)	0, 1, 2 ,3, 4, 5 wt%	DGEBA/MeTHPA	Increasing with increasing CB content		Optimal concentration of 2 wt% prodcued an increase of 32% in tensile strength, 89% in flexural strength, and 10% in impact strength. Higher and lower concentrations showed lesser improvements.		
Kim (2008)	conductive carbon black (35nm)	0, 0.5, 1, 1.5, 2, 2.5, 3 wt%	DGEBA/polyetheramine				K_{1c} increased with increasing CB content up to a maximum increase of 23% at 3 wt%	

5.2.3 Graphene

Graphene is composed of a single layer of sp-2 bonded carbon atoms that form a hexagonal pattern. A pure sheet of graphene has only carbon atoms and is highly conductive. It is also one of the strongest and stiffest materials in the world. While it is only one atom thick, its in-plane dimensions can be significantly larger (on the order of microns). Graphite is composed of multiple layers of graphene and graphite oxide contains not just carbon sheets, but also hydroxyl, epoxide and carbonyl groups bonded to the carbon atoms.

Wang et al [38] experimented with graphene and silane functionalized graphene to understand the impact on tensile stiffness and strength on a polyamide cured DGEBA epoxy. They used 1 wt% graphene and functionalized graphene and found that the functionalization further improved the mechanical properties. Both stiffness and strength improved, but the best improvement was for the functionalized graphene with a 50% improvement in strength and a 9% improvement in stiffness. They attributed the additional improvement for the functionalized graphene to the silane preventing stacking leading to improved dispersion and a stronger interfacial interaction between the silane and the epoxy. While they did not report any T_g experiments, they did find an improvement in thermal degradation properties.

King et al [39] incorporated graphene at various concentrations into a diethyltoluenediamine (DETDA) cured DGEBF epoxy and explored the impact on mechanical properties. While they saw a monotonic increase in stiffness with increasing graphene content, the tensile strength went the opposite direction. At 6 wt% graphene,

they found a 24% improvement in tensile stiffness but a 54% reduction in tensile strength. Because graphene is conductive, they also reported a significant reduction in the electrical resistivity for graphene concentrations in excess of 1 wt%. For 1 wt% there was only a very slight reduction in resistivity, with a small 4% improvement in modulus but a 27% reduction in strength.

Ribeiro et al [40] added exfoliated graphite (EG) and triethylenetetraamine (TETA) functionalized graphite oxide (GO-TETA) to TETA hardened DGEBA epoxy. The glass transition temperature and the hardness of composites made from both nanoparticles at concentrations of 0.5, 1, and 3 wt% were compared to the neat epoxy. They saw a significant improvement in the T_g, as much as 19 °C for both the 3 wt% exfoliated graphite and 1 wt% TETA functionalized graphite oxide. Other concentrations also showed significant increases but not quite as much (10 – 17 °C). This group also used nanoindentation to calculate the elastic modulus at different penetration depths. They found nearly a 10% increase for both EG and GO-TETA at depths of 300 and 600 nanometers, but a much smaller change at a depth of 1.3 microns. Values of Vickers hardness also showed significant increases with added nanoparticles of both types.

Zaman et al [41] looked at the effect on thermal and mechanical properties of adding graphene nanoplatelets (GnP) to DGEBA epoxy cured by polyoxypropylene and DGEBA cured by 4,4'-diaminodiphenyl sulfone (DDS). They looked at 4 different vol%: 0.244, 0.489, 0.984, and 1.988%. They found that increasing the concentration of GnP caused an increase in stiffness, but a decrease in tensile strength. The increases in Young's modulus for the highest concentrations (1.988 vol%) of both epoxy systems

were about 10-15%, while the reductions in strength were about 45-55%. At the lowest concentration level (0.244 vol%), the strength reduction for the polyoxypropylene cured epoxy was about 5% (with a 3% increase in modulus), while the strength reduction for the DDS cured epoxy was about 28% (with an 8% increase in modulus). However, even at the lowest concentrations, the T_g showed a significant increase of about 15 °C for both epoxy systems, with only a minimal change in resistivity (in fact the reported resistivity of the polyoxypropylene system increased). Both systems showed significant and monotonically increasing fracture toughness with increasing nanoplatelet concentration.

In an earlier study by the same lead author (Zaman) [42], the group added graphene platelets (GP) and graphene platelets modified by 4,4'-methylene diphenyl diisocyanate (m-GP) to a DGEBA epoxy with a polyoxyalkyleneamine curing agent. They used concentrations of the nanoplatelets at 1, 2.5, 4, and 5.5 wt%. Similar to the other experiment they found an increase in stiffness and a reduction in tensile strength with the addition of the graphene; however, in this experiment there was an optimal concentration level (lower than the maximum tested level) that produced the best increase in stiffness. In the case of GP, 2.5 wt% produced a 25% improvement in stiffness while 4 wt% m-GP produced a 22% increase. Higher concentrations achieved lesser levels of improvement. At the optimized concentration levels, the T_g was improved by 8 °C for GP and 12 °C for m-GP.

Based on these results, it seems graphene can increase the glass transition temperature and improve the stiffness and toughness of an epoxy. The results are generally significant. Strength, however, seems to be reduced by the addition of

graphene. With the exception of one study, all of the experiments that reported on strength showed a large decrease, worsening with an increase in graphene content.

Table 5-3. Graphene Epoxy Nanocomposites

Author (Year)	Nanoparticle(s)	Concentrations	Epoxy System	T_g	Stiffness	Strength	Toughness	Other
Wang (2012)	Graphene, Silane functionalized graphene	1%	DGEBA/Polyamide		9% improvement for functionalized graphene	Significant improvements in strength: Graphene 36%; functionalized graphene about 50%		
King (2013)	Graphene (15 um avg. diam, 7nm thick)	0, 1, 2, 3, 4, 5, and 6 wt%	DGEBF/DETDA		Increasing with increasing graphene content up to 24% at 6 wt%	Decreasing with increasing graphene content up to 54% reduction at 6 wt%		Significant reduction in electrical resistivity above 1 wt% graphene
Ribeiro (2013)	Exfoliated graphene; graphite oxide functionalized with TETA	0, 0.5, 1, 3 wt%	DGEBA/TETA	Significant increases in T_g up to 19 °C for 3 wt% exfoliated graphene and 1 wt% TETA functionalized graphite oxide. Minimum of 10 °C increase for other concentrations	Modulus as determined by nanoindentation increased at depths of 300 and 600 nm, but showed little change at a depth of 1.3 um			Nanohardness was reduced with the addition of the graphene and functionalized graphene, but the Vickers hardness showed a significant increase.
Zaman (2012)	Graphene	0, 0.244, 0.489, 0.984, and 1.988 vol%	DGEBA/polyoxypropylene and DGEBA/DDS	Significant increases in T_g, especially at very low vol%: 15 °C for both epoxy systems at 0.244 vol% graphene	Modulus increased with increasing vol% of graphene: up to 13% for polyoxypropylene system and 12% for DDS system at 1.988 vol%	Significant reduction in strength with increasing particle content, up to 47% for polyoxypropylene system and 55% for DDS system at 1.988 vol%	Improvement of up to 70% for polyoxypropylene system and 167% for DDS system at 0.984 vol%. Lesser improvement at higher and lower concentrations.	
Zaman (2011)	Graphene and MDI modified graphene	0, 1, 2.5, 4, and 5.5 wt%	DGEBA/polyoxyalkylenea mine	T_g improvements of 8 °C for 2.5 and 4 wt% graphene and 14 °C for 2.5 wt% modified graphene	Modulus incresed 25% at 2.5 wt% graphene and 22% at 4 wt% modidifed graphene. Lesser improvements above and below these optimal concentrations	Reduction in tensile strength with increasing filler content up to about 22% loss at the highest concentrations.	Significant improvements in toughness up to the optimal concentration levels of 2.5 and 4 wt% for the graphene and modified graphene systems respectively.	

5.2.4 Nanoclay

Nanoclays are layered mineral silicates. Montmorillonite (MMT), one of the common nanoclays used in studies, has a theoretical chemical formula of $(OH)_4Si_8Al_4O_{20}\cdot nH_2O$ [43]. Magnesium (Mg) can sometimes replace some of the aluminum atoms. MMT is made of 2 tetrahedral sheets surrounding an octahedral sheet [44]. Layers one nm thick can cleave off to form exfoliated nanoparticles under proper dispersion conditions [45]. This creates nanoparticles with a very high aspect ratio.

Becker et al [46] investigated the effect of octadecyl ammonium ion-modified montmorillonite layered silicate (nanoclay) on the thermal and mechanical properties of 3 different types of epoxy: DGEBA, triglycidyl p-amino phenol (TGAP), and tetraglycidyl diaminodiphenylmethane (TGDDM), all hardened with DETDA. They used concentrations of 2.5, 5, 7.5, and 10 wt%. They found that T_g was reduced with the addition of the nanoclay and higher concentrations produced more significant reductions. With 10 wt% nanoclay, the T_g was reduced about 15 °C for DGEBA and TGAP and about 20 °C for TGDDM. The mechanical properties, however showed significant improvement. The flexural modulus increased with increasing clay content for all 3 epoxies, with the improvement very similar on a percentage basis. At the highest concentration of 10 wt%, the improvement was about 20% for all 3 systems. Similarly, the toughness was improved as evidenced by the K_{1c} increasing 100% for the DGEBA and TGDDM epoxies; the TGAP system only improved about 10% at the same concentration.

On the other hand, Ratna et al [47], found an increase in T_g using DGEBA, DETDA and the same nanoclay as Becker [46] with 2.5 and 5 wt% nanoclay. Both of these researchers used similar preparation techniques with the following exceptions: Becker used an excess of epoxy in order to avoid what was reported as a detrimental effect of non-reacted amine groups while Ratna used a stoichiometric amount of hardener and Ratna also added a sonication step to the mixing process. Ratna found an increase in the T_g of 11 °C and 22 °C at 2.5 and 5 wt% respectively, compared with reductions of 2-3 °C for the same concentrations found by Becker [46]. Both groups used Dynamic Mechanical Analysis to identify the T_g.

Thelakkadan et al [48] added cloisite 30B, a nanoclay, to a DGEBA epoxy hardened by polyoxypropylene diamine and examined the effect on T_g and dielectric breakdown strength. They found that while the T_g was improved, it was not directly correlated with the amount of nanoclay. In fact, for the concentrations that varied between 0.5 to 10 wt%, the T_g improvement was generally about 10 °C. On the other hand, the dielectric breakdown strength showed a steady improvement up to 5 wt% nanoclay, but then the improvement dropped off significantly at 10 wt%. At 5 wt% the improvement in dielectric breakdown strength was 14%.

Wang et al [49] explored lower nanoclay concentrations using silane modified montmorillonite in a DGEBA epoxy cured with DDS. They used concentrations of only 1, 2 and 3 wt% and found significant differences in thermal and mechanical properties depending on the concentration. For T_g, the 1 wt% nanocomposite produced an increase in T_g of 10 °C, while the higher concentrations produced a decrease. For strength, the 2

wt% composite produced the best result of a 25% improvement over the neat system, but the other nanocomposites also produced significant improvements. Stiffness on the other hand increased nearly linearly with increasing modified clay content up to a 13% improvement at 3 wt%.

Zaman et al [50] investigated the impact of modifying montmorillonite with a polyether(mono)amine and a polyether(di)amine and adding the nanoparticles to a DGEBA epoxy and polyoxypropylene hardener. They used a nominal nanoparticle content of 2.5 wt%. In both systems, they found a small increase in T_g with the diamine system having a better improvement of 7 °C. In stiffness and toughness, the diamine modified system produced a better improvement (16% for stiffness and 58% for toughness) than the monoamine modified system (10% for stiffness and 44% for toughness). The strength for both nanocomposites showed a decrease from the neat epoxy system, with the monoamine system dropping 18% and the diamine system showing a 7% worsening. Thus in all cases the diamine system performed better.

In other studies, Garea et al [51] looked at functionalizing the nanoclay with monoamine and diamine adducts. They found a decrease in T_g with increasing modified nanoclay content (from 5 wt% up to 30 wt%) in a DGEBA epoxy hardened by polyoxypropylene diamine. Xu [52] et al compared the T_g for montmorillonite (clay), polystyrene-co-methyl acrylate modified clay (PSMA) and polystyrene-co-acrylic acid modified clay (PSAA) with an unfilled DGEBA/DDM epoxy system. They used 3 wt% of clay and found a small increase in T_g in all the systems with clay, with the largest increase of about 6 °C from the PSAA system.

From these studies, there is no definitive answer as to whether nanoclay increases or decreases the glass transition temperature. Even with the same materials, researchers found conflicting results [46,47]. In general the changes were significant (often greater than 10 °C). For stiffness and toughness, there were more consistent results. Nanoclay improves the stiffness of the epoxy system and higher concentrations produce larger improvements. Toughness was also improved by the incorporation of nanoclay. Only two of these studies looked at strength: one saw an increase and the other a decrease. Thus, there seems to be an opportunity for additional studies that clarify the variations found in these studies.

Table 5-4. Clay Nanocomposites

Author (Year)	Nanoparticle(s)	Concentrations	Epoxy System	T_g	Stiffness	Strength	Toughness	Other
Becker (2002)	octadecyl ammonium ion-modified montnorillonite (interlayer spacing 2.3 nm)	0, 2.5, 5, 7.5, 10 wt%	DGEBA, TGAP, and TGDDM with DETDA	Decreasing with increasing nanoclay content. Decreases of about 15 °C for DGEBA and TGAP and about 20 °C for TGDDM at 10 wt% nanoclay	Flexural stiffness increased with increasing clay content. All three systems showed roughly a 20% improvement at 10 wt%		Improved toughness with increasing clay content. DGEBA and TGDDM improved about 100% with 10 wt% nanoclay while TGAP only showed a 10% improvement at 10 wt%	Falling Dart Impact Test: Increasing impact energy with increasing nanoclay content up to 57% improvement at 5 wt%
Ratna (2003)	octadecyl ammonium ion-modified montmorillonite	0, 2.5, 5 wt%	DGEBA/DETDA	Increasing with increasing nanoclay content. 11 °C increase at 2.5 wt% and 22 °C increase at 5 wt%				
Thelakkadan (2012)	magnesium aluminum silicate platelets (C30B)	0, 0.5, 1, 2, 3, 5, and 10 wt%	DGEBA/polyoxypropylene diamine	Roughly a 10 °C increase in T_g, but similar improvements for all concentrations				Dialectric breakdown strenght improved up to 5 wt% but only a very small improvement at 10 wt %. At 5 wt% improvement was 14%.
Wang (2006)	montmorrilonite modified by 3-aminopropyl-timethoxysilane	0, 1, 2, 3 wt%	DGEBA/DDS	10 °C increase in T_g for 1 wt%, but a 3 and 10 °C decrease for 2 and 3 wt%, respectively	Increasing with increasing clay content up to a 13% improvement at 3 wt%	Increased about 20% for all 3 concentrations.	K_{1c} increased with addition of modified clay. Best was 77% improvement at 2 wt%	
Zaman (2011)	montmorillonite modified with ethanolamine, polyetheramine and polyetheramine (diamine)	0, 2.5 wt% of modified clay	DGEBA/polyoxypropylene	Small increase for the polyetheramine (3 °C) and polyetherdiamine (7 °C) sytems	Increase of 10% for the monoamine polyehteramine system and 16% for the diamine system	Decrease of 18% for the monamine polyetheramine and 8% for the diamine system	Increase of 44% for the monoamine polyehteramine system and 58% for the diamine system	
Garea (2008)	montmorillonite modified with monoamines and diamines	5, 15 and 30 wt%	DGEBA/polyoxypropylene diamine	Decrease in T_g with increasing modified nanoclay content. Note no baseline (0 wt%) T_g values given, but a decrease in Tg at 5 wt% from the neat value given in other papers with the same epoxy system can be inferred.				
Xu (2011)	montmorillonite, polystyrene-co-methyl acrylate modified clay (PSMA) and polystyrene-co-acrylic acid modified clay (PSAA)	0, 3 wt%	DGEBA/DDM	Small increase in T_g for the nanoclay systems with the largest increase of 6 °C for the PSAA system				

5.2.5 Alumina

Alumina (Al_2O_3) nanoparticles are spherical. Being an oxide, they are non-conductive. The alumina nanoparticles in the studies summarized below were in the range of 20-80 nm.

Zabihi et al [53] studied the impact of 50 nm alumina particles on the T_g of a DGEBA epoxy hardened with poropane diamine. They found a significant increase in T_g at the low wt% nanocomposites. The 1 wt% sample showed an increase of 20 °C; the 2.5 wt% sample had an increase of 17 °C. The higher wt% nanocomposites showed lesser improvements with the 10 wt% sample increasing 9 °C and the 15 wt% sample increasing only 4 °C.

Omrani et al [54] examined the impact of 50 nm alumina particles on the T_g and flexural stiffness of a DDM hardened DGEBA epoxy. They found that the optimal concentration was 2 parts per hundred resin (phr). This concentration showed an 8 °C increase in T_g and a 13% improvement in flexural stiffness. Both lower and higher concentrations showed lesser improvements. In a similar study [55], Omrani used the same 50 nm alumina, DGEBA, and a TETA hardener. In this study, they found that T_g only improved for the lowest 0.5 phr alumina nanocomposites, while it decreased for higher concentrations. However, in this study, the flexural modulus increased 60% at 2 phr, a much more significant result.

Jiang et al [56] looked at the effects of adding 80 nm alumina to a DDM hardened DGEBA epoxy. They looked at concentrations between 1 and 4 wt % and found an improvement in T_g of about 11 °C for all concentrations. They also found a reduction in

the CTE for all concentrations with the reduction becoming more significant with higher concentrations. In both the glassy and rubbery regions of the composites, the CTE was reduced by about 5% at 4 wt% of alumina.

Jin et al [57] added 20 nm alumina nanoparticles to DGEBA epoxy cured with DDM. They looked at concentrations from 5-15 wt% and found that the T_g, the CTE and the storage modulus were all improved by adding alumina. The best T_g increase was 10 °C for the composite with 10 wt% alumina. For the storage modulus and the CTE, the improvements increased with the concentration of alumina. The CTE was reduced 11% in the glassy region and 6% in the rubbery region at 15 wt%. The storage modulus increased 58% in the glassy region for the same highest concentration tested.

From this set of experiments, it can be seen that alumina can improve the properties of DGEBA epoxy. In general, the T_g can be increased with certain concentrations providing a significant increase of 10-20 °C. Stiffness also seems to improve with higher concentrations providing more significant reinforcement. Similarly, the CTE can be improved (reduced) by adding alumina nanoparticles.

Table 5-5. Alumina Nanocomposites

Author (Year)	Nanoparticle(s)	Concentrations	Epoxy System	T_g	Stiffness	Strength	Toughness	Other
Zabihi (2012)	Alumina 50 nm	0, 1 ,2.5, 5, 10, 15 wt%	DGEBA/poropane diamine	Significant increase at low wt%; lesser improvements at high wt%. Tg increased 20 C at 1 wt%				
Omrani (2009)	Alumina 50 nm	0, 0.5, 2, 5 phr	DGEBA/DDM	Increase at all concentrations. Largest increase was 8 C at 2 phr	Increase in flexural modulus. Best increae was about 13% at 2 phr			
Omrani (2009-2)	Alumina 50 nm	0, 0.5, 2, 5 phr	DGEBA/TETA	Tg increased slightly for 0.5 phr alumina, but decreased for higher concentrations. Increase was about 5 C at 0.5 phr and the decrease was about 7 C at 5 phr	Flexural modulus increased with addition of alumina. Best result was an increase of about 60% at 2 phr			
Jiang (2012)	Alumina 80 nm	0, 1, 2, 3, 4 wt%	DGEBA/DDM	All concentrations showed similar improvements of about 11 C				CTE reduced with increasing alumina concentrations. At 4 wt%, the CTE was reduced by about 5%.
Jin (2012)	Alumina 20 nm	0, 5, 10, 15 wt%	DGEBA/DDM	All concentrations showed an improvement of 8-10 C, with 10 wt% showing the largest increase of 10 C	Storage modulus in the glassy region increased with increasing alumina content. Improvement was 58% at 15 wt% alumina			CTE reduced with increasing alumina concentrations. At 15 wt%, the CTE was reduced by about 11% in the glassy region and 6% in the rubbery region

5.2.6 Carbon Nanotubes

Carbon nanotubes can be thought of as a rolled up sheet or sheets of graphene. They have the same hexagonal pattern of carbon atoms, but instead of lying in a flat sheet, they form a tube. A single walled carbon nanotube (SWCNT) has only one tube and is one of the stiffest and strongest known materials. Multi-walled carbon nanotubes (MWCNT) are made of two or more concentric tubes held together by Van der Waals forces. Because the inner tubes can slide out, the MWCNTs provide less mechanical reinforcement.

Many researchers have studied the incorporation of CNTs into epoxies to improve thermal and mechanical properties. To further improve the properties, many scientists have tried functionalizing the nanotubes in order to improve the interfacial properties between the nanotubes and the epoxy.

Zhou et al [58] added multi-walled carbon nanotubes to a DGEBF epoxy hardened with an aromatic amine. The nanotubes had a diameter of 30-60 nm and a length of 3-10 microns and were incorporated at a concentration of 0.1, 0.2, 0.3 and 0.4 wt%. They found that the flexural modulus increased with increasing concentration of MWCNTs up to a 12% increase at 0.4 wt%. However, the flexural strength was optimized at 0.3 wt% with an improvement of 28%. Fracture toughness also reached its peak at 0.3 wt% with an improvement in K_{1c} of about 30%. The authors did not report on the T_g of the epoxy nanocomposites, but did note a small increase of about 2 °C for a woven carbon fiber epoxy system by adding 0.3 wt% MWCNTs.

Hsieh et al [59] added larger MWCNTs with a diameter of 120 nm and a length of 140 microns to a MHHPA hardened DGEBA epoxy to explore the impact on toughness, stiffness and T_g. They utilized concentrations of 0.1, 0.2, and 0.5 wt% and found that toughness and stiffness improved with higher concentration levels. K_{1c} and G_{1c} increased by 42% and 68% respectively at a concentration level of 0.5 wt%. Stiffness also increased with increasing concentrations up to 12% at 0.5 wt%. However, they reported a small decrease in the T_g with higher concentration levels. The T_g dropped about 3 °C at 0.5 wt%. In looking at transmission optical microscopy images of the composites, the authors noted significant agglomerations of nanotubes which may explain the drop in T_g.

Karripal et al [60] researched the effect of adding 60-90 nm MWCNTs, both with and without predispersion in acetone, to DGEBA epoxy with a polyamidoamine (PAA) hardener. They used concentrations of 2, 4, 6, and 8 wt% and looked at the impact on T_g and electrical resistivity. The T_g increased with increasing MWCNT content up to a maximum improvement of 10 °C for 8 wt% MWCNT with no predispersion. For the MWCNTs predispersed in acetone, the improvements in T_g were consistently slightly less at the same concentration levels. Interestingly, they found that SEM images of the epoxy nanocomposites showed better dispersion of the MWCNTs when they were predispersed in acetone, in spite of these reported impacts on the T_g. On the electrical resistance side, however, the resistivities dropped more for the predispersed MWCNTs. Higher concentrations led to more significant decreases, but all nanocomposites tested showed a significant drop even at the lowest concentrations reported.

Thakre et al [61] compared the impact of adding SWCNTs and a conductive grade CNT mixture of SWCNTs, DWCNTs, and MWCNTs (with some extraneous carbon black and metal elements) to a DGEBF epoxy with an aromatic diamine curing agent. With the conductive grade CNTs costing much less than SWCNTs, they were trying to identify a more economical method of improving material properties. They examined the changes in T_g and electrical conductivity at concentrations of 0.0015, 0.0225, and 0.03 wt%. Other than the 0.03 wt% concentration of conductive grade CNTs, they found significant increases of 11-20 °C in the T_g for the epoxy nanocomposites, with the largest increases of 20 °C for the 0.03 wt% SWCNT and 0.0225 conductive grade CNTs. Interestingly, the 0.03 wt% conductive grade CNTs only produced a 4 °C increase in T_g. Electrical conductivity showed a significant increase starting at 0.015 wt% for SWCNTs and at 0.0225 wt% for the conductive grade CNTs.

Guadagno et al [62] examined the effect of different dispersion approaches on the T_g, elastic modulus, and electrical conductivity of adding 0.5 wt% MWCNTs to a DGEBA epoxy with a DDS curing agent with a BF_3 accelerant. Three different approaches were used to combine the nanoparticles with the epoxy: a ball miller, an ultrasonic probe, and a magnetic stirrer. All mixing approaches produced a significant increase in T_g, with the magnetic stirrer and the ultrasonification both producing improvements of 14 °C. The ultrasonicated nanocomposite also produced an increase of about 30% in the elastic modulus at 40 and 60 C, and about 60% at 150 C, while the other dispersion methods showed produced little change in the modulus. The researchers also found a dramatic increase in conductivity upon adding the MWCNTs.

Hosur et al [63] explored the impact of different mixing methods and concentrations of MWCNTs on the strength, stiffness, and T_g of a DGEBA epoxy cured with a tetra aliphatic amine. Concentrations levels of 0.2 and 0.4 wt% were incorporated using a centrifugal mixer, a shear roller, and a solvent based approach in combination with the 2 mixing approaches. In general, they found a small increase in both flexural strength and stiffness. The best strength improvement of 20% came from the 0.4 wt% sample incorporating all three mixing methods. This same concentration and mixing approach produced an 11% improvement in flexural modulus. All concentrations and mixing techniques showed an improvement in T_g from 8-12 °C.

Other researchers experimented with functionalized nanotubes in order to improve the interfaces between the epoxy and the nanotubes. Jin et al [64] incorporated 1 wt% MWCNTs into a DGEBA epoxy with a DDM curing agent. This group explored the different impacts of pure, acid treated (sulfuric and nitric), and acid followed by dodecyl amine treated MWCNTs on the T_g, storage modulus, and toughness properties. While there was a small increase of 3 °C in T_g for the pure MWCNT epoxy nanocomposite, the acid treated and amine treated MWCNTs produced an improvement of 9 and 11 °C respectively. Fracture toughness as measured by K_{1c} also showed improvements with the best improvement of 38% achieved with the amine functionalized MWCNTs. The storage modulus, however, showed the reverse pattern with decreases for all of the nanocomposites with the amine functionalized composite showing the largest decrease of about 5%.

Jeong Tai Kim et al [65] incorporated non-functionalized and silane (3-APTES) functionalized MWCNTs into a DGEBA epoxy with a polyamidoamine hardener (PAA). The MWCNTs were 10-15 nm in diameter and were added at 0.5 wt% to identify the impact on T_g, flexural strength and flexural modulus. The unmodified MWCNTs produced a 3 °C increase in T_g while the silane functionalized MWCNTs produced a 7 °C increase. Both flexural strength and flexural modulus followed this same pattern: an improvement for the non-functionalized MWCNTs, and a larger improvement for the functionalized ones. The silane functionalized MWCNTs showed a 13% improvement in stiffness and a 17% improvement in strength. In a similar study by the same group, Hee-Cheul Kim et al [66] utilized the same materials, but included concentrations of 0.1, 0.2, 0.3, 0.4, along with the previously tested 0.5 wt%. They found the optimal concentration for improving T_g was 0.3 wt % which produced an increase of 7 °C for non-functionalized and 13 °C for silane functionalized MWCNTs. Tensile strength was little impacted by unmodified MWCNTs, but 0.3 wt % silane functionalized MWCNTs produced an increase of 15%. The tensile modulus continued to increase with additional MWCNT content, with the modified MWCNTs demonstrating better improvements. The best result was an increase in tensile modulus of 66% at 0.5 wt% functionalized MWCNTs.

Silva et al [67] functionalized MWCNTs with acid followed by TETA and looked at the impact on T_g on a DGEBA epoxy hardened with TETA. They found a significant increase in T_g of 18 °C for both 0.5 and 1.0 wt % nanocomposites for the functionalized MWCNTs. For non-functionalized MWCNTs, they found an increase of 15 °C for 0.5

wt% but only a 3 °C increase of 1 and 3 wt%. They attributed this falloff to agglomerations at higher concentrations.

Prado et al [68] chose to use melamine to add NH_2 groups to the surface of MWCNTs and DWCNTs to investigate the impact on a DGEBA epoxy with an amine hardener. They used a CNT concentration of 0.075 wt%. While they found small declines in T_g of 3 °C and 2 °C for non-functionalized MWCNTs and DWCNTs respectively, the functionalized nanotubes produced an increase of 5 °C and 9 °C respectively.

Thus, in general, CNTs can significantly improve the T_g of various epoxy systems. There is often an optimal concentration of CNTs that produces the most significant result and functionalizing nanotubes can also lead to a better result. Unlike some of the other nanoparticles, CNTs seem to improve strength and stiffness properties at the same time. Concentration levels are again important. Electrical conductivity is drastically increased as well above certain concentration levels.

Table 5-6. Carbon Nanotube Nanocomposites

Author (Year)	Nanoparticle(s)	Concentrations	Epoxy System	T_g	Stiffness	Strength	Toughness	Other
Zhou (2008)	MWCNT (diam 30-60 nm, length 3-10 um)	0, 0.1, 0.2, 0.3, 0.4 wt%	DGEBF/aromatic amine	Neat epoxy not reported. Very small increase of 2 C reported for weave carbon fiber epoxy composite with 0.3 wt% MWCNT	Flexural stiffness Increased with increasing concentration of MWCNT up to 12% at 0.4 wt%	Flexural strength increased with increasing concentration of MWCNT up to 28% at 0.3 wt%, but then fell off to 19% improvement at 0.4 wt%	K1c increased with MWCNT concentration to a max increase of about 30% at 0.3 wt%	
Hsieh (2011)	MWCNT	0, 0.1, 0.2, 0.5 wt%	DGEBA/MHHPA	Slight decreasein Tg with increasing concentration. 3 °C drop at 0.5 wt%.	Increasing with increasing concentration of MWCNT up to 12% at 0.5 wt%		Kc and Gc improvements up to 42 and 68% increases respectively at 0.5%	
Karippal (2009)	MWCNT (60-90nm, 1-3 um)	0, 2, 4, 6, 8 wt%, with and without predispersion in acetone by ultrasonication	DGEBA/polyamidoamine (PAA)	Improvement in Tg with increasing MWCNT content. Best result was 10 C improvement for 8 wt% MWCNT with no acetone predipersion				Electrical resistivity dropped significantly for the smallest MWCNT loading and continued to drop with increasing loading
Thakre (2009)	SWCNT and XD-CNT (electrical grade consisting of SW, DW, MW CNTs and some impurities	0, 0.015, 0.0225, 0.03 wt%	DGEBF/aromatic diamine	Improvement in Tg for both types of nanotubes at all concentrations, with a 20 C improvement at 0.03 wt% SWCNT and 0.0225 Wt% XD-CNT. At 0.015 wt% XD-CNT, there was a 12 C improvement in Tg				Significant reductions in electrical resistivity began to occur at 0.015 wt% for SWCNTs and 0.0225 wt% for XD-CNTs
Guadagno (2010)	MWCNT (10 nm, 0.1-10 um), dispersed by different methods	0, 0.5 wt%	DGEBA/DDS	Significant increase of 9-14 °C depending on dispersion method.	Improvement of about 28% for ultrasonication; other dispersion methods showed scattered results depending on test temperature			Electrical resistivity significantly reduced at concentrations as low as 0.1 wt%
Hosur (2010)	MWCNT (8-15nm, 10-50 um)	0, 0.2, 0.4 wt%	DGEBA/tetra aliphatic amine	Increase in Tg for all mixing techniques and concentration up to 12 C for 0.4% wt	Improvements in flexural stiffness up to 13% for 0.4 wt%	Most concentrations and dispersion methods showed an improvement in flexural strength. The best was about a 20% improvement for 0.4 wt% that incorporated solvent, centrifugal mixing, and 3 roll mixing.		
Jin (2011)	MWCNT (diam 10-20 nm, length 20-50 um), pure, acid treated, and acid treated followed by functionalization with amine	0, 1 wt%	DGEBA/DDS	Small increase for pure MWCNTs. More significant increase of 9-11 C for acid treated and amine treated respectively	Storage modulus reduced with MWCNTs, and further reduced with acid treatement and then functionalization		K1c increased with MWCNTs and further increased with acid treatment and then functionalization	
Kim (2009)	MWCNT (10-15 nm; silane functionalized and non-functionalized)	0, 0.5 wt%	DGEBA/polyamidoamine (PAA)	Increase of 3 C for non-functionalized and 7 C for silane functionalized MWCNT composites	Both functionalized and non-functioanlized MWCNT nanocomposites showed an improvement in flexural stiffness, with a larger 13% improvement for the functionalized MWCNTs	Both functionalized and non-functioanlized MWCNT nanocomposites showed an improvement in flexural stiffness, with a larger 17% improvement for the functionalized MWCNTs		
Kim (2010)	MWCNT (10-15 nm; silane functionalized and non-functionalized)	0, 0.1, 0.2, 0.3, 0.4, 0.5 wt%	DGEBA/polyamidoamine (PAA)	Increase in Tg for both functionalized and non-functionalized MWCNTs. Functionalized MWCNTS showed better improvement. Optimal result was at 0.3 wt% for both functionalized and non-functionalized, with an 11 C increase for functionalized and a 6 C increase for non-functionalized	Improvement in tensile stiffness with increasing MWCNT content. Functionalized MWCNTs showed more significant improvement up to 66% at 0.5 wt%	Tensile strength showed modest improvement for functionalized MWCNTs up to 0.3 wt%. At 3 wt% there was a 15% improvement in strength. Other concentrations and non-functionalized MWCNTs showed little change		Dispersion was better for the functionalized MWCNTs leading to the better themral and mechanical properties.
Silva (2014)	MWCNT (diam 10-40 nm length 1-25 um) and functionalized with TETA	0, 0.5, 1.0, 3.0 wt%	DGEBA/TETA	Significant increase at 0.5 wt% MWCNT and 0.5 & 1.0 wt% MWCNT functionalized with TETA				
Prado (2009)	DWCNT and MWCNT, with and without melamine modification	0, 0.075 wt%	DGEBA/amine	9 C and 5 C increase in Tg for melamine treated DWCNTs and MWCNTs, respectively. Small decrease for untreated DWCNTs and MWCNTs				

5.3 Summary of Chapter 5

While research results are not always consistent, some generalizations can be made about the impact of adding specific nanoparticles to epoxy systems. Silica generally improves the toughness of the epoxy, but has mixed results on the strength, stiffness and T_g. There are a limited number of studies of carbon black with epoxy, but preliminary results show a significant improvement in T_g. Graphene studies show an improvement in T_g, stiffness, and toughness, but a reduction in strength. Studies on nanoclay show a stiffness and toughness improvement, but inconsistent results for T_g and strength. Alumina studies generally show improvements in T_g and stiffness, but the studies reviewed for this paper did not include any results for strength or toughness. Studies with carbon nanotubes frequently showed improvements in Tg, strength, and stiffness.

CHAPTER 6 IMPACT OF NANOPARTICLES ON THE THERMAL AND MECHANICAL PROPERTIES OF A MODIFIED CYCLOALIPHATIC EPOXY

6.1 Introduction

As just discussed in the previous chapter, nanoparticles can have a significant impact on the thermal and mechanical properties of epoxy systems. Due to various factors including different epoxy systems, varying concentrations of nanoparticles, diverse functionalization or basic nanoparticle properties and manufacturing methods, and new approaches to disperse the particles, results from study to study are not always consistent. Due to their less common use and higher cost, there has also been very little research on cycloaliphatic epoxy nanocomposites. However, cycloaliphatic epoxies offer significant advantages in high voltage applications, such as higher T_g and resistance to ozone [5]. Thus, it was endeavored to conduct experiments to determine the impact of nanoparticles on the thermal and mechanical properties of cycloaliphatic epoxies.

The findings in Chapter 2 demonstrated that a coating could significantly reduce the chemical aging on the surface of the hybrid composite rod used in ACCC conductors. However, in both Chapter 2 and Chapter 3 it was seen that physical aging of the epoxy

still had a detrimental effect on the flexural properties of the rods. Physical aging increased the residual stresses in the composite components of the rods [6] and these reductions led to reduced flexural properties. Therefore, the goal of the nanoparticle experiments was to identify a nanoparticle and a concentration level that would significantly impede physical aging. Because physical aging increases as the temperature approaches T_g [6,8], the initial approach was to find a nanocomposite with an increased T_g; thus, operating the conductor at a given temperature would place it further below its glass transition temperature.

Of course, nanoparticles, as seen in the previous chapter, do not only impact the glass transition temperature; other material properties are affected as well. Therefore it is necessary to test the nanocomposites for changes in mechanical properties that could affect the performance of the hybrid composite rods. Properties that are important in the resin include tensile strength, stiffness, and elongation at failure; flexural strength, stiffness, and strain at failure; and electrical conductivity, especially in the glass fiber epoxy composite region which serves as a galvanic reaction barrier between the aluminum and the carbon fiber epoxy composite region. For example, using too much of a conductive nanoparticle, in excess of the percolation threshold, can reduce the effectiveness of the galvanic reaction barrier.

Nanoparticles impact material properties in various ways. For example, on the mechanical front, nanoparticles can change the stiffness of a material through load transfer by means of covalent or weak van der Waals bonds. Physical aging in polymers such as epoxies occurs through the movement and reconformation of polymer chains to a

lower energy state (which also leads to reduction in free volume in the polymer) [8]. The removal of van der Waals bonds allows the components of the polymer chains to reorient through the rotation or change in conformation of its various bonds. These reorientations allow the chains to slide and move to a lower energy state. However, thermal energy is needed for both the melting of the van der Waals bonds (leading to a rubbery state, not a full melting of the polymer) and for the rotation of the bonds. This thermal energy is supplied when the polymer is heated.

While it has not been proven precisely how nanoparticles can impact physical aging and the glass transition temperature, there are several ways that can be envisioned. Any process that hinders the rotation of bonds or the movement of chains will raise the glass transition temperature; conversely, an arrangement that enhances movement or rotation could reduce the T_g.

A nanoparticle in an epoxy could mechanically block the rotation of a chain, hindering its movement and raising the glass transition temperature. On the other hand, a soft nanoparticle could act like a plasticizer and allow for easier rotation of polymer bonds, thereby reducing the T_g. In the event that there is covalent bonding between the nanoparticles and the polymer (see Chapter 7), the nanoparticle could act as a cross-linker and thus block movement of the chains. A nanoparticle could also be pictured as a barrier between polymer chains leading to additional free volume and easier rotation of bonds. Additionally, any van der Waals bonding between the nanoparticles and the polymer chains could have higher or lower energies than the van der Waals bonds between the chains themselves, leading to higher or lower thermal energy requirements to melt these

bonds. Thus the nanoparticles can impact the glass transition temperature of the epoxy systems.

Experiments were therefore conducted to try to identify an optimal nanoparticle and concentration level that could protect against physical aging and preserve other important mechanical properties.

6.2 Experimental

6.2.1 Materials

Two different epoxy systems were used. One was graciously supplied by Lindau Chemicals and the other by CTC Global. The Lindau system was a cycloaliphatic epoxy, Lindoxy 190, with an anhydride hardener, LS 252. The CTC Global system was similar to, but not exactly the same as, the system used in the actual manufacturing of ACCC rods. It, too, was a cycloaliphatic epoxy with an anhydride hardener. Middleton et al [5] demonstrated that the two resin systems are very similar.

Based on the results from Chapter 5, three different types of nanoparticles were selected to be added to the epoxy systems: graphene, silica, and carbon black. Researchers at Michigan Technological University (MTU) including Danielle Klimek-McDonald and Dr. Julie King performed the actual manufacturing of the nanocomposites to support this research.

Two different graphenes were used, M-5 and TC-307. Graphene M-5 was supplied by XGsciences and consists of short stacks (6-8 nm) of graphene nanoplatelets with an average particle diameter of 5 microns [69]. The M-5 was used in combination

with the Lindau epoxy system. For the CTC resin system, Asbury TC307 Graphene Nanoplatelets were used. These nanoplatelets are about 1 micron in diameter [70].

Two types of silica were also used. With the Lindau systems, Aerosil A200 (average particle size 12nm) fumed silica was incorporated while in the CTC Resin a proprietary silica from Cabot was used. Three proprietary carbon blacks, labeled CB1, CB2, and CB3, also from Cabot, were included in the CTC resin system.

Base concentrations of 1 wt% of nanoparticles were applied for all three types of nanoparticles and some variations were then manufactured and tested depending on initial results.

6.2.2 Experiments

Various thermal, mechanical, and electrical tests were conducted at both MTU and at the University of Denver to characterize the impact of adding nanoparticles.

Dynamic Mechanical Analysis (DMA) on a TA Instruments Q800 DMA was performed at both sites (Composite Technology Development graciously allowed the use of their TA Q800 DMA for samples tested in Denver). The glass transition temperature was determined based on the maximum of the tan δ. At MTU, a single cantilever setup was used with a sample size of 3 mm thick, 12 mm wide and 35 mm long, with the clamp distance 17.5 mm. The temperature was swept from 50 °C to 290 °C at 3 °C per minute with an amplitude of 30 μm and a constant frequency of 1 Hz. At DU, a dual cantilever setup was used with sample sizes of 52 mm long, 13 mm wide, and 3 mm thick with the clamp distance of 35 mm. The temperature was swept from 35 °C to 290 °C at 5 °C per minute with an amplitude of 15 μm and a frequency of 1 Hz. Comparative samples of

neat CTC resin analyzed at DU and MTU showed negligible differences in the determined T_g.

Tensile tests were conducted at MTU according to ASTM D638 utilizing a InstruMet Sintech screw-driven mechanical testing machine and standard tensile test specimens. Flexural tests were conducted at DU utilizing a MTS 858 Table Top System test frame with a 3-point bend fixture. Samples were 61 mm long, 12.7 mm wide, and 3.2 mm thick. The test fixture had support pins with a spread of 50.8 mm. Samples were loaded at a constant crosshead displacement of 1 mm / minute and measurements were taken of displacement and load until failure. Electrical tests were conducted at MTU using 3 mm thick disks with a diameter of 6.4 cm in a Keithley 6517A Electrometer/High Resistance Meter with an 8009 Resistivity Test Fixture.

6.3 Results and Discussion

Table 6-1 lists the results of the tests conducted on the various epoxy nanocomposites. In this table, green indicates an improvement in properties with respect to the application in hybrid composite rods while red indicates a worsening. For example, a decrease in resistivity is labeled as a worsening since it reduces the impact of the galvanic reaction barrier. Of course, in other applications, creating a more conductive polymer may be considered beneficial. Due to a limited number of samples, not all tests were conducted on all epoxy/nanoparticle composites.

Table 6-1. Summary of Test Results on Epoxy Nanocomposites

Resin	Particle	Conc. (wt%)	Ultimate Tensile Stress (MPa)	Strain at Ultimate Tensile Stress (%)	Tensile Fracture Stress (MPa)	Strain at Tensile Fracture Stress (%)	Tensile Modulus (MPa)	Ultimate Flex Strength (Mpa)	Strain	Flex Modulus (Mpa)	Tg °C	Electrical Resistivity (Ω-cm)
Lindoxy 190/LS-252	-	-	**47.86**	**3.42**	**47.86**	**3.42**	**2094**	**85.66**	**5.59**	**2238**	**248.0**	
Lindoxy 190/LS-252	Graphene M-5 xGnP	1.0	40.75	2.45	40.75	2.45	2140	63.97	3.41	2181	252.0	
Lindoxy 190/LS-252	Silica A200 FS	1.0	46.63	3.26	46.63	3.26	2027	78.71	5.43	2076	251.0	
Lindoxy 190/LS-252	Silica A200 FS (sonicated)	1.0	46.76	3.29	46.76	3.29	2014	71.90	5.38	1888		
Lindoxy 190/LS-252	Silica A200 FS (sonicated)	4.0	44.10	3.10	44.10	3.10	2106	76.31	6.18	1996		
CTC	-	-	**56.27**	**4.01**			**2040**				**241.0**	**9.65E+16**
CTC	Graphene TC307	1.0	50.49	3.66			2040				241.3	
CTC	Graphene TC307	2.0	50.93	3.71			2070				239.5	
CTC	Graphene TC307	3.0	48.65	3.35			2080					
CTC	Graphene TC307	4.0	42.78	2.81			2100				240.2	2.09E+14
CTC	CB1	1.0	49.49	4.22			1920				235.6	2.06E+14
CTC	CB2	1.0	50.43	4.01			2070				236.6	5.81E+10
CTC	CB3	1.0	46.84	3.27			2000				233.1	7.74E+11
CTC	CB1	0.5										
CTC	CB1	2.0										
CTC	Silica	1.0										

As noted in the prior chapter, results from incorporating nanoparticles are highly varied and may depend on dispersion, concentrations, functionalization, specific type of nanoparticle, size of nanoparticles, type of epoxy, and other factors. Even in highly experienced laboratories, results may not always be necessarily consistent.

Recalling that the goal was to raise the T_g while preserving the other properties, these initial forays into epoxy nanocomposites cannot be considered successful, but they are informative.

Only three of the tested epoxy nanocomposites showed any increase in T_g in comparison with the neat epoxy systems: 1 wt% silica and 1 wt% M-5 graphene in the Lindau resin system and 1 wt% Graphene TC307 in the CTC system. However these increases were minor with the maximum increase only 4 °C for the M-5 graphene. All other nanocomposites showed minor to moderate decreases (1-8 °C) in T_g.

For graphene epoxy nanocomposites tested in this study, T_g showed only modest changes. Aside from the small increase noted above, there was little impact on this property at 1, 2, and 4 wt% concentrations when tested with the CTC system. These results are different from those found in studies reviewed in the prior chapter, where in general, there was an improvement in the glass transition temperature. In the current study, tensile strength showed a significant drop with the inclusion of graphene but in general a small increase in stiffness. Higher loadings of graphene led to less strong but more stiff nanocomposites. These results are consistent with those in prior studies. Seemingly, there is load transfer to the graphene particles to improve the stiffness, but there may be stress concentrations around the sharp particles that lead to reduced

strength. The electrical resistivity at 4 wt% showed a 2 order of magnitude reduction from the neat epoxy, but still was an electrical insulator at 2.09 E14 ohm-cm.

For the three 1 wt% carbon black nanocomposites, there was a meaningful drop in T_g, 6-8 °C. This result differs with that found in the literature noted in the prior chapter, where significant improvements were seen. However, there were only two studies found that looked at the impact of carbon black on the glass transition temperature of epoxies and neither of these used a cycloaliphatic epoxy system. The carbon blacks utilized for this dissertation also diminished the tensile strengths of the epoxy, but had only minor impact on the stiffness, with CB2 having a minor increase while CB1 and CB3 had minor decreases. The electrical resistivities of all three carbon black composites dropped, but were still in the insulating range, meaning that the percolation threshold was not yet met.

Silica may be the best candidate of the three as the 1 wt% nanocomposite showed a slight 3 °C increase in Tg with only a minor drop in strength and stiffness. Other researchers had found mixed results in Tg, strength, and stiffness as noted in Table 5-1. Since silica is non-conducting, higher loadings may be possible which could lead to different results.

Looking at the results from the property point of view produces some useful insights. From the strength standpoint, all of the nanocomposites showed reduced strength, but silica performed the best. Graphene TC307 and CB2 showed roughly equivalent results. Higher loadings of graphene further reduced the strengths. On the stiffness side, the results were generally opposite: silica performed the worst with a reduction in stiffness, while graphene (both M-5 and TC307) showed an improvement.

CB2 again performed the same as TC307, while the other two carbon black formulations showed a slight worsening in strength. On T_g, 1 wt% loadings of graphene produced small increases and higher graphene loadings produced small reductions. 1 wt% Silica produced a small increase and 1 wt% of all three carbon blacks produced moderate decreases.

6.4 Summary of Chapter 6

Incorporating nanoparticles into epoxy systems produces changes in mechanical and thermal properties. For some properties such as stiffness, general composite techniques, such as the rule of mixtures, are effective as predicting the changes in material properties, provided there is enough load transfer to the reinforcing nanoparticle. For other properties such as Tg or strength, the task is not as simple. Much remains to be learned about the mechanisms that create changes in these bulk properties in the nanocomposites. Research conducted by others and research conducted in this study reinforce this issue. This study has attempted to produce nanocomposites with improved properties, but has not succeeded.

Two approaches can be taken moving forward. More types, concentrations, combinations, or functionalizations of nanoparticles or different dispersion methods could be manufactured and tested, but this is a very tedious process. A different approach would be to try to understand the interactions between nanoparticles and the epoxy polymer in order to better predict resulting properties. The next chapter explores one way of doing this: looking at the fundamental interactions of epoxy and graphene.

CHAPTER 7 AB INITIO MODELING OF THE INTERACTION BETWEEN GRAPHENE AND THE COMPONENTS OF A CYCLOALIPHATIC EPOXY SYSTEM

7.1 Introduction

While finite elements models break a material into small components in order to understand the interactions of pieces of the material and molecular dynamics models look at the interactions at the atomic level using an applied potential to understand the interactions between atoms, ab initio calculations go a full level deeper. These quantum chemical computations analyze interactions at a sub-atomic level, utilizing the nuclei and electrons of all of the atoms. It makes no a priori assumptions about bonds, but instead calculates the energy of the electrons and the atomic nuclei, utilizing the interactions among all of these subatomic particles. There are five components of the total energy of the system: the kinetic energies of all of the electrons (Te), the kinetic energies of all of the nuclei (Tn), and the potential energies created by the electrical interactions of all pairs of nuclei (Unn), all pairs of an electron and a nucleus (Uen), and all pairs of electrons (Uee). Bonds are formed if the lowest energy geometrical configuration of the atoms produces nearby atoms with an electron buildup between them to act as the glue.

Computational chemistry programs try to numerically solve the Schrödinger equation and produce a configuration that minimizes the total energy of a system. Because the systems that are being analyzed in this research are generally stable, it is assumed that Tn is negligible (the Born-Oppenheimer assumption [71]). While the kinetic energy of the electrons, the nuclei-nuclei repulsions, and the electron-nuclei attractions are somewhat straight-forward to calculate, the electron-electron repulsions are much more time consuming to calculate.

In this study Gaussian 09 [72], a commercially available computational chemistry package, was utilized to calculate the energies of three base molecules as well as the energies produced by all three pairs of two of the molecules when chemically bonded. Additionally, the transition state for the bonding reaction was determined in order to analyze the activation energy required for the bonding reaction. The three molecules utilized were: graphene (with hydrogen caps on the edges), a cycloaliphatic epoxy monomer (3,4-Epoxycyclohexylmethyl 3, 4-Epoxycyclohexane Carboxylate), and nadic methyl anhydride (NMA, 8-Methyl-4-oxatricyclo[5.2.1.02,6]dec-8-ene-3,5-dione). These three molecules are presented in Figure 7-1, Figure 7-2, and Figure 7-3 respectively.

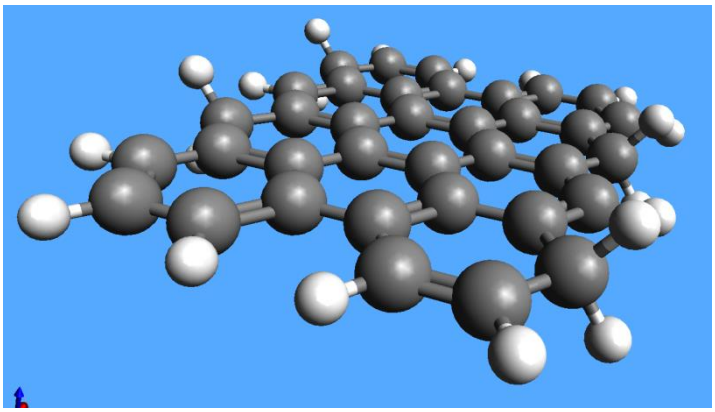

Figure 7-1. Graphene

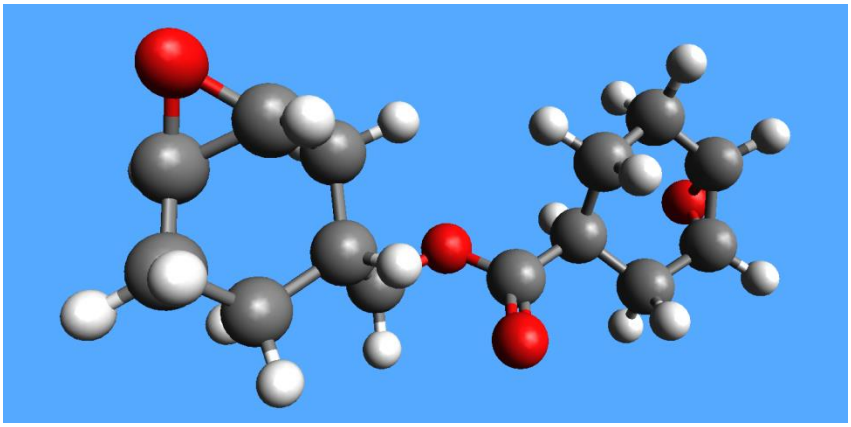

Figure 7-2. Cycloaliphatic epoxy monomer

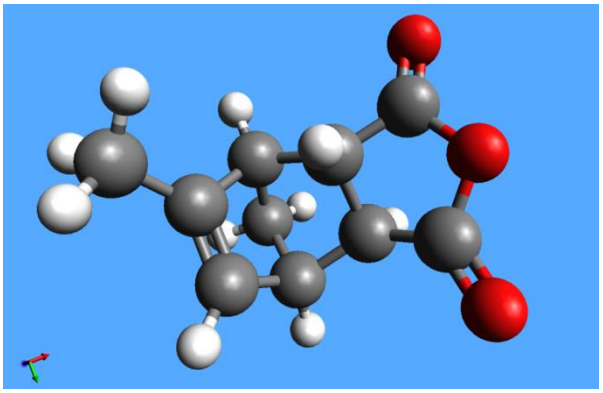

Figure 7-3. Nadic methyl anhydride (NMA)

7.2 Modeling Approach

To determine the likelihood of chemical bonds being formed between molecules in a mixture of graphene nanoparticles, cycloaliphatic epoxy monomers, and NMA, the curing agent, several steps needed to be taken. First, the energies of the base molecules were calculated using the semi-empirical approach AM1 in Gaussian 09. Then, three pairings of the molecules were considered: 1) cycloaliphatic epoxy with NMA, 2) cycloaliphatic epoxy with graphene, and 3) NMA with graphene.

The first step in a polymer cross linking chain reaction is the hydroxylization of one of the component molecules. For the cycloaliphatic epoxy with NMA case, NMA was chosen to be hydroxylated. Thus a hydroxyl group was added to the NMA molecule, splitting the ring and leaving two free hydroxyl end groups (see Figure 7-4). The energy of this new molecule was calculated. Then the appropriate crosslinking bond was formed to create an NMA-cycloaliphatic molecule (Figure 7-6) and again the energy was calculated. The difference between the energy of the crosslinked molecule and the sum of the energies of the hydroxylated NMA and the cycloaliphatic monomer as stand-alone molecules is the bond stabilization energy or simply the bond energy.

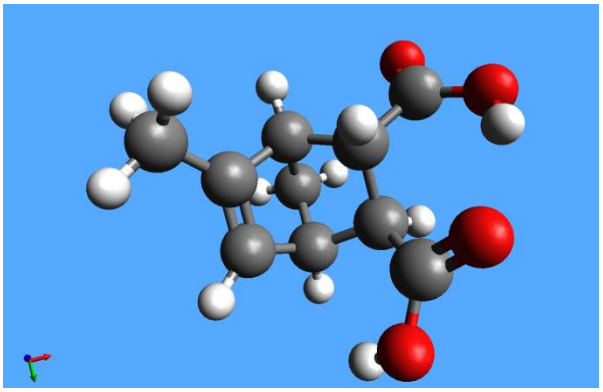

Figure 7-4. Hydroxylated NMA

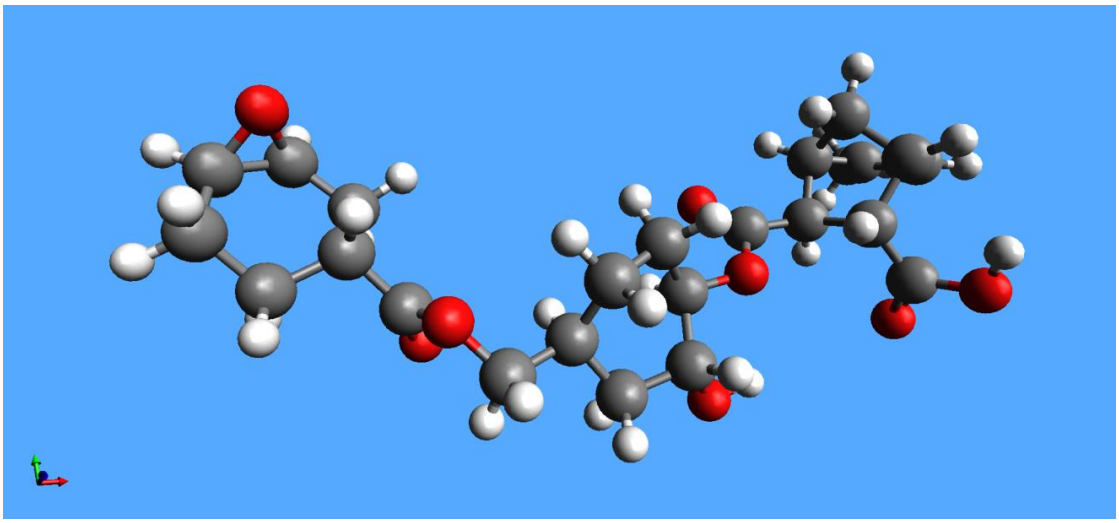

Figure 7-5. Covalently bonded cycloaliphatic epoxy and NMA

For the remaining two reactions, the graphene sheet was hydroxylated, with one hydroxyl group on each side of the sheet (see Figure 7-5). Note that commercially available graphene is not 100 % carbon. For example, M-5 graphene's carbon content is about 99.5% [69]; thus it is likely to have some oxygen based groups such as hydroxyl groups as pendants. These hydroxyl sites then become potential ring-opening bonding sites when interacting with either a cycloaliphatic epoxy or an NMA molecule. The energy of the hydroxylated graphene was calculated as well as the energy of each of the two bonded molecules (see Figure 7-7 and Figure 7-8). The stabilization energy for the graphene cycloaliphatic

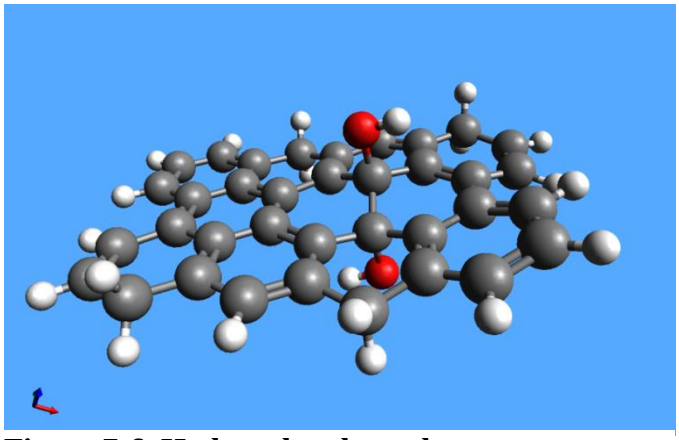

Figure 7-6. Hydroxylated graphene

epoxy bond and the graphene NMA bond was then calculated as the differences between the energies of the bonded molecules and the sum of each pair of starting reactants.

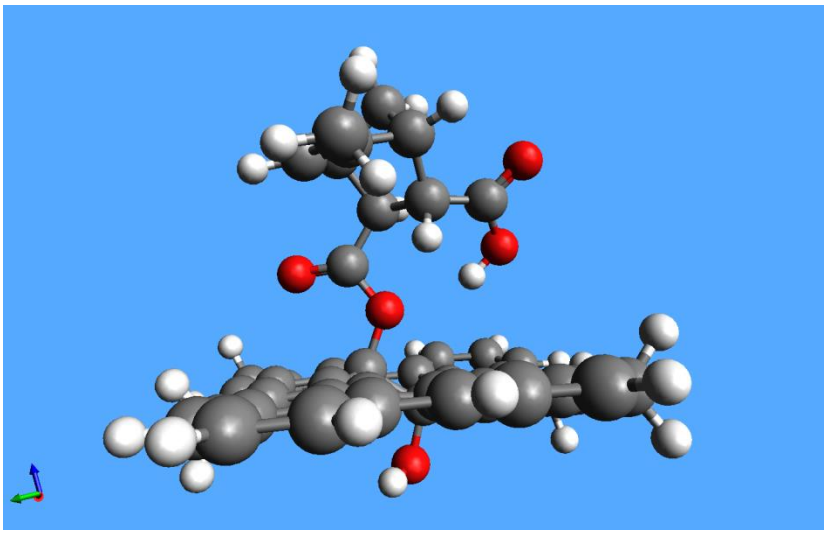

Figure 7-7. NMA covalently bonded to hydroxylated graphene

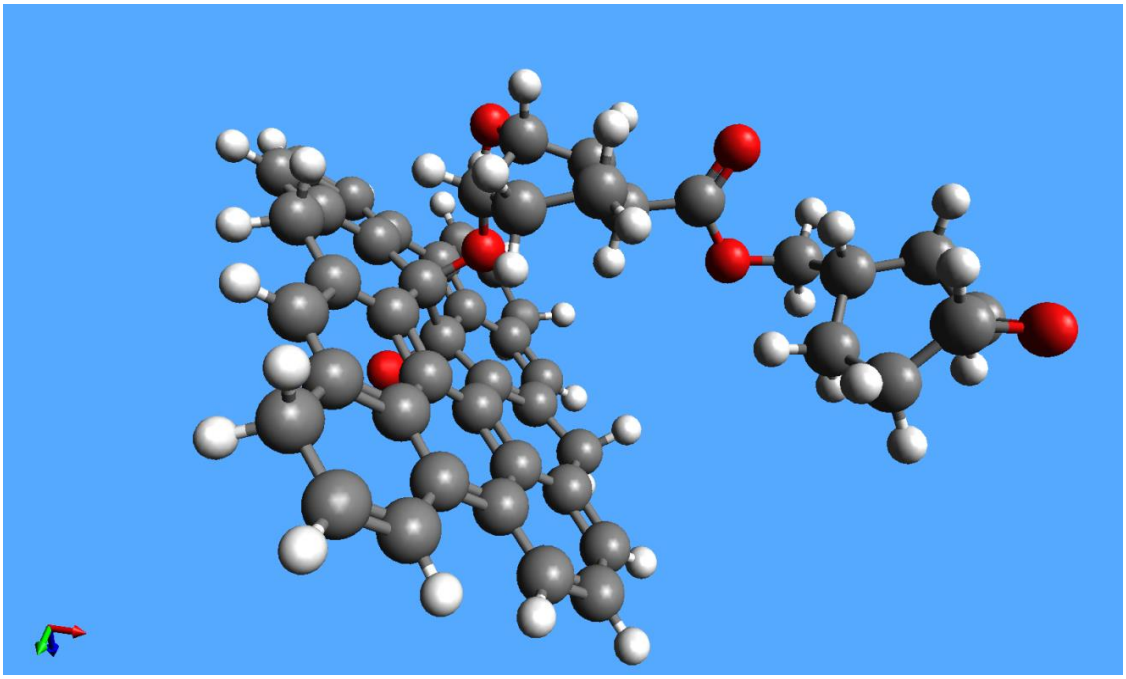

Figure 7-8. Cycloaliphatic epoxy monomer covalently bonded to hydroxylated graphene

However, there is one other factor to be considered. In a chemical reaction, the reaction path passes through a transition state (Figure 7-9). This transition state is almost always at a higher energy level than the sum of the energies of the reactants. This increase in energy is known as the activation energy. The higher the activation energy, the more energy required to allow the reaction to proceed. In the curing reaction discussed here, this energy comes from heat. Additionally, a bonding reaction can be reversed. Generally the dissociation reaction follows the reverse path of the bonding reaction, but if the bond energy is significant, then the activation energy for the dissociation reaction is considerably higher than the activation energy of the bonding reaction and is less likely to occur, leaving a considerable likelihood of the bond to remain in place. Thus the likelihood of having a bonded molecule is based on both the bond energy and the activation energy.

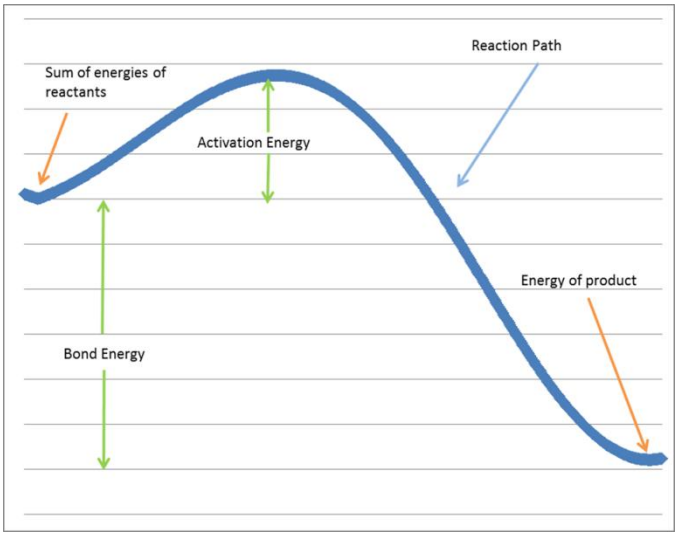

Figure 7-9. Activation and Bond Energy

Gaussian 09 provides the capability of finding the geometry and energy of a transition state given a starting state, an ending state, and, optionally, a guess at the transition state. To confirm that a transition state has been found, it is necessary to check that there is one and only one imaginary vibrational frequency in the transition state.

Having a single imaginary vibrational frequency indicates that the transition state is a minimum in the potential energy surface of the geometry of the molecule in all but one direction where it is a maximum. Thus there is a saddle point for the reaction path.

Using the QST3 option in Gaussian 09, the transition states for all three pairings of molecules (all three potential bonding reactions) were calculated. Thus both the bond energies and the activation energies were calculated. The transition states are depicted in Figure 7-10, Figure 7-11, and Figure 7-12.

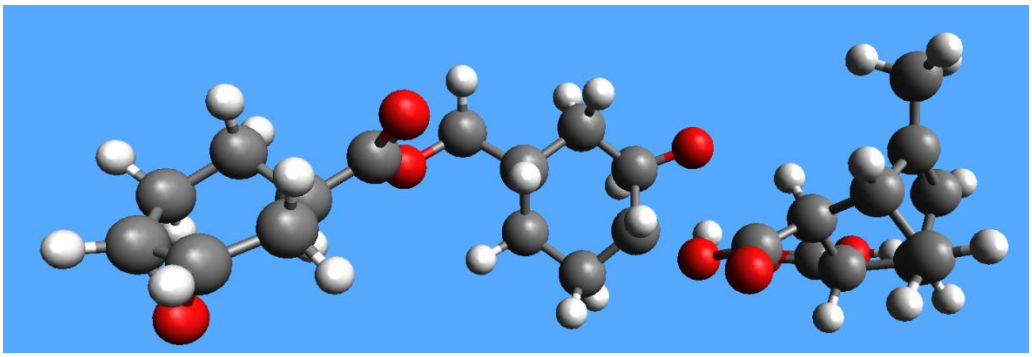

Figure 7-10. Transition state for cycloaliphatic epoxy and NMA

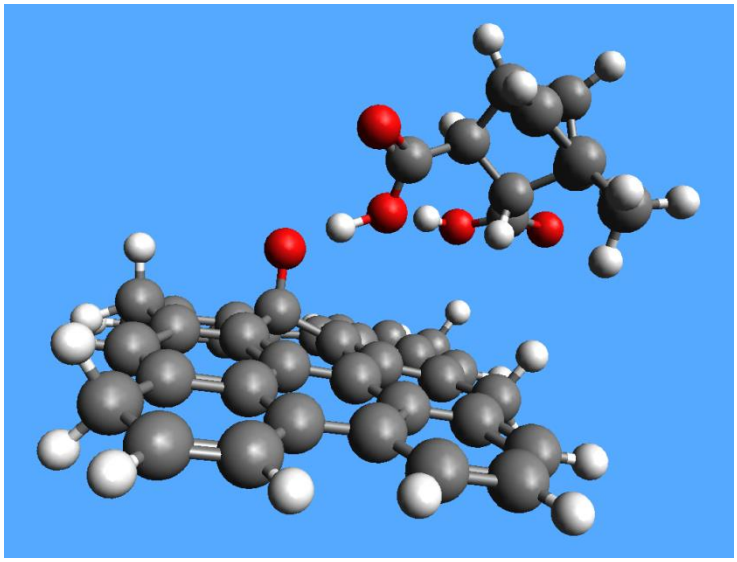

Figure 7-11. Transition state for graphene and NMA

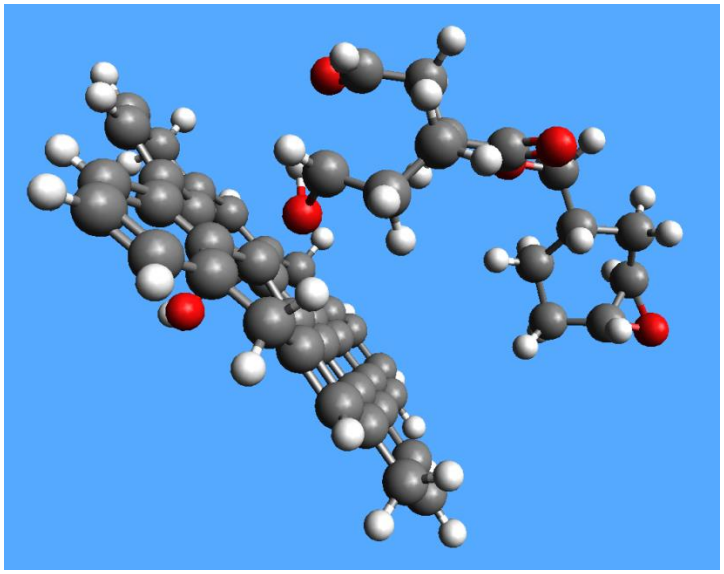

Figure 7-12. Transition state for graphene with cycloaliphatic epoxy

7.3 Results and Discussion

The results of the calculations are shown in Table 7-1. The bonding of the epoxy system components, NMA and the cycloaliphatic epoxy, showed the greatest bond energy and the lowest activation energy. However, with a curing cycle that includes temperatures of 200 °C, it is more than likely that there is the possibility of covalent bonding between NMA and graphene, provided some of the graphene has hydroxyl groups.

Table 7-1. Bond energy and activation energy of pairings of molecules

	NMA/ Cycloaliphatic Epoxy			**Graphene with Cycloaliphatic Epoxy**			**Graphene with NMA**	
		kcal/mole			kcal/mole			kcal/mole
A	Cycloaliphatic Monomer	-87.4	A	Cycloaliphatic Monomer	-87.4	A	NMA Monomer	-41.3
B	NMA Monomer	-41.3	B	Graphene	149.4	B	Graphene	149.4
C	Hydroxylated NMA	-154.4	C	Hydroxylated Graphene	86.9	C	Hydroxylated Graphene	86.9
D	Hydroxylated NMA/Cycloaliphatic Monomer	-315.2	D	Hydroxylated Graphene/ Cycloaliphatic Monomer	-29.8	D	Hydroxylated Graphene/NMA Monomer	4.0
E	Transition State	-231.2	E	Transition State	63.6	E	Transition State	74.1
(A+C)-D	**Bond Energy**	**73.4**	(A+C)-D	**Bond Energy**	**29.3**	(A+C)-D	**Bond Energy**	**41.6**
E-(A+C)	**Activation Energy**	**10.6**	E-(A+C)	**Activation Energy**	**64.1**	E-(A+C)	**Activation Energy**	**28.5**

7.4 Summary of Chapter 7

While this chapter analyzes one possible interaction between graphene nanoparticles and a specific cycloaliphatic epoxy, much research remains to be performed in the field of nanocomposites to fully understand the mechanisms that lead to changes in thermal and mechanical properties. Not all nanoparticles will form covalent bonds with all resin systems. However, as noted in Chapter 5, many different nanoparticles can

impact the performance of various epoxies. Thus there are other interactions and mechanisms in play which need to be researched in order to be fully understood and in order to design optimal systems.

CHAPTER 8 GENERAL DISCUSSION AND FINAL CONCLUSION

New polymer core HTLS conductors can transmit 2-3x the amount of current through the same size and weight transmission lines as traditional aluminum and steel (ACSR) lines. In order to reach this level of transmission, however, the lines must be operated at temperatures much higher than used for ACSR. The genesis of this research came from a simple manufacturer claim that the hybrid composite rods containing unidirectional glass and carbon fibers in an epoxy matrix could operate at 180 ^{0}C for an indefinite period of time [1]. Burks and Kumosa [4] found this not necessarily to be the case: aging at 180 ^{0}C under atmospheric conditions for twelve months significantly and dramatically reduced the flexural properties of composite rods. Thus, this dissertation set out to find approaches to reduce the impact of thermal aging on polymer based composites using innovative multiscale approaches both experimentally and numerically.

Initially, the degradation mechanisms in the hybrid rods were not fully understood. While there was definite aging of the composites, the specific reasons why the reductions in properties slowly progressed in the first nine months of aging, followed by a dramatic dropoff after twelve months was not known. Middleton et al [6] modeled the effect of thermal aging on the residual stresses in the glass fiber and carbon fiber sections of the composite and found significant buildup with increases in both time and aging temperature due to physical aging of the epoxy. This research gave a clue as to

what could be the cause of the initial slow but persistent reduction in flexural properties during the first nine months, but did not explain the rapid reduction after 9 months.

The early part of the research for this dissertation set out to try to understand if the rapid dropoff in properties between nine and twelve months could be reduced or eliminated. It was hypothesized that chemical aging through thermal oxidation of the surface was responsible for this reduction. Applying a barrier coating to the surface of the rods as described in Chapter 2 demonstrates that there truly is a different mechanism in play. While there remained a slow and continuing decline in the flexural properties of the rods during the first nine months of aging, there was no dramatic decline after twelve months.

To support the hypothesis that chemical aging can change the initiation point and source of failure in the uncoated rods after thermal aging, a finite elements model was built. While this simple model utilized a microscopic notch instead of a sharp crack, it was an innovative approach that demonstrated that stress concentrations at the tip of the notch are sufficient to create a new location where shear stresses are at a maximum in the composite materials of the rod. These stress concentrations, however, do not fully explain the similar dramatic reduction in flexural stiffness seen after twelve months. There are several possible causes of this decline in modulus. One theory is that the residual stresses in the composites between nine and twelve months of aging created enough damage to the interface throughout the bulk of the material that the load transfer from the matrix to the fibers was severely compromised. This would explain the 14% drop in flexural modulus. However, optical and SEM imaging of the composites utilized in this research

did not reveal any noticeable interfacial damage. Additionally, had this physical aging been the source of the dramatic decline, the same result should have been seen in the coated rods, but it was not. Therefore, it was presented that the surface damage to the rods through chemical oxidation was sufficient to reduce and eliminate the mechanical contribution of enough of the outer region of the rods to produce this dramatic reduction in stiffness. An analytical model was then developed that showed that the damage would need to be about 270 microns in thickness which was a little larger than the approximately 150 micron oxidation depth that Barjestah et al [3] found in their aging experiment. Thus, Chapter 2 was a proof of concept that a coating that can significantly reduce surface oxidation can delay the onset of the dramatic dropoff in flexural properties of the hybrid composite rods. While the fluoropolymer material used was effective under the laboratory conditions, it might not survive the operating conditions that would be experienced in-service. For example, this kind of material will likely not maintain its full protection when subjected to fretting conditions from Aeolian vibrations or other degrading conditions experienced in service. Therefore, in future research, experiments will need to be designed and conducted to test this coating and if necessary to identify other materials with similar protective capabilities that are able to withstand the extreme environment in which the conductors operate.

Chapter 3 explored the impact of an even higher aging temperature (200 ^{0}C) on the performance of the rods and the coating. It was assumed that the higher temperature would speed thermal aging, both chemical and physical. Physical aging seemed to follow the expected pattern: the flexural load at failure dropped more at each aging duration than

the corresponding result at 180 ^{0}C for both the coated and the uncoated rods. The results followed the pattern of increasing residual stresses modeled by Middleton et al [6] for higher temperatures and longer durations. However, the chemical aging did not seem to follow the theorized pattern. Instead of a dramatic decline before twelve months of aging for the uncoated rods which would have occurred if the chemical aging had also been accelerated by the higher temperature, there was in fact no decline up to and including twelve months for either the uncoated or the coated rods. There was also no reduction in the flexural modulus through twelve months. Thus, the chemical aging impact seemed to have been significantly reduced at the higher temperature. This initially perplexing result was eventually resolved by integrating results from Barjestah et al [3] who found that oxidation thickness into the transverse surface of the rod was not as deep for 200 ^{0}C as for 180 ^{0}C for the same aging times. Their analysis showed that while the rate of diffusion of oxygen into the epoxy increased with increasing temperature, the rate of consumption of the oxygen (reaction with the epoxy) grew at an even faster rate and therefore the oxygen did not penetrate as far into the polymer matrix. Therefore the surface damage would be limited.

This reduced depth of damage at higher temperatures combined with the required damage depth for diminished stiffness calculated in Chapter 2 is consistent with the maintained flexural stiffness at 200 ^{0}C. However, there remains an open question as to whether limiting the thickness of the surface damage also impedes the development of microcracks of sufficient size and sharpness to limit any dropoff in flexural load at failure. It might have been expected that the stiffness would be maintained, but the load

at failure for the uncoated rods still would show a dramatic dropoff at some point in time. Future research will need to be performed to continue to understand all of the mechanisms in play.

It is also interesting to note that at all aging durations at both 180 ^{0}C and 200 ^{0}C (with the exception of twelve months at 180 ^{0}C when chemical aging is presumed to have impacted the results for the uncoated rods), the coated rods had a slightly lower (7-20%, with an average reduction of 12%) load at failure than the uncoated rods. This could be a coincidence due the scatter of the results, or it could indicate that something involved in the coating process weakens or damages the rods slightly. In the coating process, the rods had been lightly sandblasted to improve the adhesion of the coating. While there were no visible defects in the fibers, there may have been microscopic damage leading to the worsened results. However, these imperfections would have been limited to the surface and may not be consistent with the hypothesis that the initiation point for failure due to physical aging occurs in the bulk of the material and not on the surface. Again, more research is needed to understand all of the complex mechanisms involved.

Chapters 2 and 3 provide significant evidence that a coating that reduces surface oxidation also significantly improves the performance of the rods when subjected to long-term thermal aging at 180 ^{0}C. However, Middleton et al [6] also showed that residual stresses increase with higher temperatures. Conversely, lowering the operating temperature would reduce the physical aging impact. Transmitting less current would reduce the resistive heating and thereby lower the operating temperature. However, this would diminish one of the advantages of the advanced HTLS conductor. Therefore, the

research in Chapter 4 was conducted to determine if a coating on the surface of the aluminum that increases its emissivity could significantly reduce the temperature of the conductor for a given level of current. A simple finite elements model was created to compare the temperature of the entire conductor with and without an enhanced emissivity coating. The results were also compared to the temperatures expected with varying levels of steady wind. The model determined the amount of resistive heating that would lead to a steady state temperature of 180 ^{0}C for the entire conductor if there were no wind and no radiative cooling. This same amount of heating was then applied with differing levels of emissivity and different wind speeds to find the new steady state temperatures. As expected, higher emissivities and higher wind speeds reduced the steady state temperatures. There was a 30 ^{0}C drop for an emissivity increase from 0.3 to 0.9. While the impact of the emissivity enhancement could be more than matched by a steady wind of 0.89 m/s (3.2 km/h), the emissivity increase would be quite beneficial on a very calm day.

An experiment was then conducted to validate the modeled results. An ACCC conductor was painted black to increase its emissivity. The black conductor and a control untreated conductor were both heated to 80 ^{0}C and then allowed to cool in a room temperature atmospheric environment. The black conductor cooled up to two times faster than the uncoated, again indicating the increase in radiative cooling and the value of an increase in emissivity. Of course, at a given wavelength of electromagnetic radiation the emissivity of an object is equal to its absorptivity; therefore the appropriate coating for

in-service use must be carefully designed to avoid increasing the absorption of energy from the sun which would be detrimental to the desired outcome.

In addition to surface coatings, the research of this thesis then explored ways of reducing the impact of thermal aging on the bulk of the polymer material utilized in the ACCC conductor. If physical and chemical aging could be retarded, the conductors could then operate at high temperatures for longer periods of time and still maintain appropriate safety margins. Therefore the research turned to identifying ways of modifying the epoxy matrix of this conductor to improve its thermal performance, while still protecting its important mechanical characteristics.

Much research in recent years has focused on the property enhancement capabilities of nanoparticle fillers. Chapter 5 is a review of recent research of the impact of various types of nanoparticles on epoxies. The goal was to identify nanoparticles that could be added to the cycloaliphatic epoxy matrix in order to increase its glass transition temperature (to slow the physical aging processes) while still protecting its strength and stiffness that are critical to its performance in the conductor rods. Six different types of nanoparticles were reviewed: silica, carbon black, graphene, nanoclay, alumina, and carbon nanotubes. In general, published research was conducted on basic epoxies such as DGEBA or on specific epoxies for a specific aeronautical application. Little research was available on cycloaliphatic systems such as those utilized in the conductor rods, but it was felt that summarizing the results would give some insights into potential candidates.

The results were somewhat sporadic and even confusing due to the use of various resin systems, concentration levels, nanoparticle functionalization approaches, and

dispersion methods. In some experiments, improvements in glass transitions temperatures were noted for specific nanoparticles, while the opposite result was presented in other papers for very similar systems. Many nanocomposite systems did not show monotonic results with increased concentration levels of nanoparticles; oftentimes there was an optimal concentration level to maximize a specific property. Carbon nanotubes showed the most promising results, but because of their high cost and complicated dispersion protocols utilized in the papers, it was decided that these would not be appropriate for a large-scale commercial solution. Therefore, of the remaining particles, the top candidates of graphene, carbon black and silica were selected for initial analysis.

Chapter 6 presents results of preliminary experiments combining nanoparticles with the cycloaliphatic epoxy system from Lindau chemicals and a system from CTC Global that is believed to be quite similar. The initial results do not yet identify a good candidate to be incorporated in the resin system. While 1 wt% graphene and silica produced a small increase in T_g, the increase was too small to be considered a major success. Additionally, there was a reduction in the other mechanical properties for these very same nanocomposite systems. However, it is still not clear whether these systems should be ruled out. The success of the dispersion approach still needs to be evaluated and if the nanoparticles are not well dispersed, other approaches need to be identified and tried. It may also be beneficial to functionalize the nanoparticles in order to get a better or different interaction with the epoxy.

In Chapter 7 the interaction of graphene with the epoxy system was studied at the ab initio level. Graphene was selected because of its prevalence in experimental research

and because it is one of the simplest systems to model using quantum chemistry which is limited in the number of atoms that can be modeled. It is noted that there needs to be oxygen based groups present on the graphene in order to get a chemical interaction (covalent bond) with the epoxy. These types of interactions can help with dispersion. Even without chemical bonds, the functional groups on the nanoparticles may help increase the van der Waals interactions between the epoxy and the nanoparticles. The value of these additional interactions may overcome what is lost in properties in the nanoparticles themselves once they are no longer pristine. For example, graphene oxide may be a better candidate for this application than graphene (and it also reduces the conductivity of the nanocomposite, thereby allowing for better maintenance of the galvanic layer). Additionally, there need to be more concentration levels tried. As noted in Chapter 5, increased weight percentages do not necessarily mean better results. Very low concentration levels of carbon black in specific epoxy systems led to big changes in material properties. Either more concentration levels need to be manufactured and tested or the ab initio approach in Chapter 7 needs to be greatly expanded in order to understand the nanoparticle epoxy interactions and therefore more intelligently identify and select candidate nanoparticles. Of course, multiscale modeling will need to come into play as the number of atoms that can be modeled with a true ab initio approach is limited by today's techniques and computing power.

Overall, this dissertation presents a broad array of innovative approaches, experimental results, and numerical analyses that lead to an improved design of polymer

matrix composites utilized in elevated temperature applications in general and specifically in polymer core composite conductors. First, a novel approach of utilizing a barrier coating that may prevent thermal oxidation was proposed and demonstrated to dramatically improve the performance of the rods after being subjected to long-term thermal aging. A unique finite elements model was developed to explain the source of the improvements in this approach and supported the newly discovered explanation of the transition from physical aging to chemical aging based damage being the source of flexural failure. The simple and effective coating approach should be commercially scalable. Secondly, it was identified that the diminution of flexural properties due to chemical aging is not as significant at an even higher temperature of 200 ^{0}C as it is at 180 ^{0}C. Again, the experimental result was supported by a numerical model and an amalgamation of results from other researchers. This discovery also reinforces the hypothesis that chemical aging is the source of the dramatic dropoff in flexural properties after 12 months of aging of the uncoated rods at 180 °C. The value of utilizing an enhanced emissivity coating to reduce the operating temperature of the conductor was proven experimentally and numerically. Lastly, significant progress was made in the evaluation of incorporating nanoparticles in the epoxy matrix to slow the physical and potentially chemical aging process and increase the in-service life of the polymer core composite conductors. The comprehensive research thus completed for this dissertation has significantly contributed to the rapid improvement, acceptance, and deployment of the polymer based HTLS conductor technology in this country and worldwide.

REFERENCES

[1] CTC Global Website. http://www.ctcglobal.com/products/accc-conductors/another-sub-page/ 6/20/2014.

[2] Kopsidas K, Rowland S. A performance analysis of reconductoring an overhead line structure. IEEE Transactions on Power Delivery; 24 (4), October 2009.

[3] Barjasteh, E., Bosze, E.J., Tsai, Y.I., Nutt, S.R. Thermal aging of fiberglass/carbon-fiber hybrid composites. Composites Part A: Applied Science and Manufacturing 40, (2009) 2038–2045.

[4] Burks, B., Kumosa, M., 2012. The effects of atmospheric aging on a hybrid polymer matrix composite. Composites Science and Technology 72, 1803–1811.

[5] Middleton, J., Burks, B., Wells, T., Setters, A.M., Jasiuk, I., Predecki, P., Hoffman, J., Kumosa, M. The effect of ozone on polymer degradation in Polymer Core Composite Conductors. Polymer Degradation and Stability 98, (2013) 436–445.

[6] Middleton, J., Hoffman, J., Burks, B., Predecki, P., Kumosa, M. Aging of a Polymer Core Composite Conductor: Mechanical Properties and Residual Stresses. Composites Part A: Applied Science and Manufacturing 69, (2015) 159–167.

[7] Burks, B., Middleton, J., Kumosa, M. Micromechanics modeling of fatigue failure mechanisms in a hybrid polymer matrix composite. Composites Science and Technology 72, (2012) 1863–1869.

[8] Odegard, G.M., Bandyopadhyay, A. Physical aging of epoxy polymers and their composites. Journal of Polymer Science Part B: Polymer Physics 49, (2011) 1695–1716.

[9] Struik, L. Physical aging in amorphous polymers and other materials. Amsterdam: Elsevier Scientific Publishing Company, 1978.

[10] Shlyapnikov, Y. A., Kiryushkin, S.G., and Marʹin, A.P.; English translation by Kazutin B. and. Shlyapnikov, Y. A. Antioxidative stabilization of polymers. Bristol, PA : Taylor & Francis, c1996.

[11] Mori, T., Tanaka, K. Average stress in matrix and average elastic energy of materials with misfitting inclusions. Acta Metallurgica 21, (1973) 571–574.

[12] Mura, T. Micromechanics of Defects in Solids. Springer Netherlands, 1987.

[13] Eshelby, J.D. The Determination of the Elastic Field of an Ellipsoidal Inclusion, and Related Problems. Proceedings of the Royal Society of London. Series A. Mathematical and Physical Sciences 241, (1957) 376–396.

[14] Performance Composites Ltd. Website. http://www.performance-composites.com/carbonfibre/mechanicalproperties_2.asp 6/30/2014.

[15] Bockarjova, M., Andersson, G., 2007. Transmission line conductor temperature impact on state estimation accuracy, in: Power Tech, 2007 IEEE Lausanne. IEEE, pp. 701–706.

[16] Gentle, J., Myers, K., Baldwin, T., West, I., Hart, K., Savage, B., Ellis, M., Anderson, P. Concurrent wind cooling in power transmission lines, in: Western Energy Policy Research Conf., Boise, Idaho (2012).

[17] Goh, 2013. Critical aging segments of power transmission line. American Journal of Engineering and Applied Sciences 6, 340–351.

[18] http://blog.opower.com/2012/09/hot-and-heavy-energy-usage-how-the-demand-and-price-for-electricity-skyrocketed-on-a-100-day/, downloaded 4/6/2015.

[19] Lee,H., Neville, K. Handbook of epoxy resins. McGraw-Hill, 1967.

[20] Napierska, D., Thomassen, L., Lison, D., Martens, J., Hoet, P. The nanosilica hazard: another variable entity. Particle and Fibre Toxicology (2010), 7:39.

[21] Vivero-Escoto, J. Silica Nanoparticles: Preparation, Properties and Uses. Nova Science Publishers Inc., New York, 2012.

[22] Zhang, H., Zhang, Z., Friedrich, F., Eger, C. Property improvements of in situ epoxy nanocomposites with reduced interparticle distance at high nanosilica content. G8Acta Materialia 54 (2006) 1833–1842.

[23] Ou, C., Shiu, M. Epoxy Composites Reinforced by Different Size Silica Nanoparticles. G8Journal of Applied Polymer Science, Vol. 115, (2010)2648–2653.

[24] Allahverdia, A., Ehsanib, M., Janpoura, H., Ahmadib, S. The effect of nanosilica on mechanical, thermal and morphological properties of epoxy coating. Progress in Organic Coatings 75 (2012) 543– 548.

[25] Tzetzis, D., Mansour, G., Tsiafis, I., and Pavlidou, E. Nanoindentation measurements of fumed silica epoxy reinforced nanocomposites. Journal of Reinforced Plastics and Composites (2013) 32: 160.

[26]Conradi, M., Zorko, M., Kocijan, A., Verpoest, I.. Mechanical properties of epoxy composites reinforced with a low volume fraction of nanosilica fillers. Materials Chemistry and Physics, Volume 137, Issue 3, 15 (2013), 910–915.

[27] Dittanet, P., Pearson, R. Effect of silica nanoparticle size on toughening mechanisms of filled epoxy. Polymer 53 (2012) 1890-1905.

[28] Sajjad, M., Feichtenschlager, B., Pabisch, S., Svehla, J., Koch, T., Seidler, S., Peterlik, H., Kickelbick, G. Study of the effect of the concentration, size and surface chemistry of zirconia and silica nanoparticle fillers within an epoxy resin on the bulk properties of the resulting nanocomposites. Polym Int 61 (2012) 274–285.

[29] Johnsen, B., Kinloch, A., Mohammed, R. Taylor, A., Sprenger, S. Toughening mechanisms of nanoparticle-modified epoxy polymers. Polymer 48 (2007) 530-541.

[30] Hsieh, T., Kinloch, A., Masania, K., Sohn Lee, J., Taylor, A. Sprenger, S. The toughness of epoxy polymers and fibre composites modified with rubber microparticles and silica nanoparticles. J Mater Sci (2010) 45:1193–1210.

[31] Zheng, Y., Chonung, K., Wang, G., Wei, P. Jiang, P. Epoxy/Nano-Silica Composites: Curing Kinetics, Glass Transition Temperatures, Dielectric, and Thermal–Mechanical Performances. Journal of Applied Polymer Science, Vol. 111, (2009) 917–927.

[32] Huang, X., Zheng, Z., Jiang, P. Influence of Nanoparticle Surface Treatment on the Electrical Properties of Cycloaliphatic Epoxy Nanocomposites. IEEE Transactions on Dielectrics and Electrical Insulation Vol. 17, No. 2; April 2010.

[33] Ragosta, G., Abbate, M., Musto, P., Scarinzi, G., Mascia, L. Epoxy-silica particulate nanocomposites: Chemical interactions, reinforcement and fracture toughness. Polymer 46 (2005) 10506–10516.

[34] http://en.wikipedia.org/wiki/Carbon_black

[35] Kosmidou, T., Vatalis, A., Delides, C., Logakis, E., Pissis, P., Papanicolaou, G.. Structural, mechanical and electrical characterization of epoxy-amine/carbon black nanocomposites. eXPRESS Polymer Letters Vol.2, No.5 (2008) 364–372.

[36] Ma, A., Chen, W., Hou, Y., Zhang, G. Dispersion, Mechanical and Thermal Properties of Epoxy Resin Composites Filled with the Nanometer Carbon Black. Polymer-Plastics Technology and Engineering, 49:9, (2010) 916-920.

[37] Kim, B., Park, S., Lee, D. Fracture toughness of the nano-particle reinforced epoxy composite. Composite Structures, Volume 86, Issues 1–3, November 2008, 69–77.

[38] Wang, X. Xing, W., Zhang, P., Song, L., Yang, H., Hu, Y. Covalent functionalization of graphene with organosilane and its use as a reinforcement in epoxy composites. Composites Science and Technology 72 (2012) 737–743.

[39] King, J., Klimek, D., Ibrahim, I., Odegard, G. Mechanical Properties of Graphene Nanoplatelet/Epoxy Composites. Journal of Applied Polymer Science 128 6 (2013) 4217-4223.

[40] Ribeiro, H., Silva, W., Rodrigues, M., Neves, J., Paniago, R., Fantini, C., Calado, H., Seara, L., Silva,G. Glass transition improvement in epoxy/graphene composites. J Mater Sci (2013) 48:7883–7892.

[41]Zaman, I., Kuan, H., Dai, J., Kawashim, N., Michelmore, A., Sovi, A., Dong, S., Luonga, L., Ma, J. From carbon nanotubes and silicate layers to graphene platelets for polymer nanocomposites. Nanoscale, 4, (2012)4578.

[42] Zaman, I., Phan, T., Kuan, H., Meng, O., La, L., Luong, L., Youssf, O., Ma, J. Epoxy/graphene platelets nanocomposites with two levels of interface strength. Polymer 52 (2011) 1603-1611.

[43] "montmorillonite." *Encyclopaedia Britannica. Encyclopaedia Britannica Online Academic Edition*. Encyclopædia Britannica Inc., 2014. Web. 12 Feb. 2014. <http://www.britannica.com/EBchecked/topic/391037/montmorillonite>.

[44] http://en.wikipedia.org/wiki/Montmorillonite

[45] http://www.sigmaaldrich.com/materials-science/nanomaterials/nanoclay-building.html

[46] Becker, O., Varley, R., Simon, G. Morphology, thermal relaxations and mechanical properties of layered silicate nanocomposites based upon high-functionality epoxy resins. Polymer 43 (2002).

[47] Ratna, D., Manoj, N., Varley, R., Singh Raman, R., Simon, G.. Clay-reinforced epoxy nanocomposites. Polym Int 52 (2003) 1403–1407.

[48] Thelakkadan, A., Coletti, G., Guastavino, F., Fina, A. Thermomechanical and electrical characterization of epoxy-organoclay nanocomposites. POLYM. ENG. SCI., 52 (2012) 1037–1046,.

[49] Wang, L., Wang, K., Chen, L., Zhang, Y., He, C. Preparation, morphology and thermal/mechanical properties of epoxy/nanoclay composite. Composites Part A 37 (2006).

[50] Zaman, I., Le, Q., Kuan, H., Kawashima, N., Luong, L., Gerson, A., Ma, J. Interface-tuned epoxy/clay nanocomposites. Polymer 52 (2011) 497-504.

[51] Garea, S., Iovu, H., Bulearca, A. New organophilic agents of montmorillonite used as reinforcing agent in epoxy nanocomposite. Polymer Testing 27 (2008) 100–113.

[52] Xu, Y., Peng, H., Wanga, X., Su, S. Comparative study of different polymerically-modified clays on curing reaction and thermal properties of epoxy resin. Thermochimica Acta 516 (2011) 13–18.

[53] Zabihi, O., Omrani, A., Rostami, A. Thermo-oxidative degradation kinetics and mechanism of the system epoxy nanocomposite reinforced with nano-Al2O3. Journal of Thermal Analysis Calorimetry 108 (2012).

[54] Omrani, A., Simon, L., Rostami, A. The effects of alumina nanoparticle on the properties of an epoxy resin system. Materials Chemistry and Physics 114 (2009) 145–150.

[55] Omrani, A., Rostami, A. Understanding the effect of nano-Al2O3 addition upon the properties of epoxy-based hybrid composites. Materials Science and Engineering A 517 (2009) 185–190.

[56] Jiang, W., Jin, F., Park, S. Thermo-mechanical behaviors of epoxy resins reinforced by nano=Al2O3 particles. Journal of Industrial and Engineering Chemistry 18 (2012) 594–596.

[57] Jin, F., Park, S. Thermal properties of epoxy resin-filler hybrid composites. Polymer Degradation and Stability 97 (2012).

[58] Zhou, Y., Pervin, F., Lewis, L., Jeelani, S. Fabrication and characterization of carbon/epoxy composites mixed with multi-walled carbon nanotubes. Materials Science and Engineering A 475 (2008) 157–165.

[59] Hsieh, T., Kinloch, A., Taylor, A., Kinloch, I. The Effect of Carbon Nanotubes on the Fracture Toughness and Fatigue Performance of a Thermosetting Epoxy Polymer. Journal of Materials Science, Vol. 46, 7525-7535, 2011.

[60] Karippal, J., Murthy, H., Rai, K., Krishna, M., Sreejith, M.. Electrical and Thermal Properties of Twin-Screw Extruded Multiwalled Carbon Nanotube/Epoxy Composites. J. of Materi Eng and Perform 19, (2010) 1143–1149.

[61] Thakre, P, Bisrat, Y., Lagoudas, D. Electrical and mechanical properties of carbon nanotube-epoxy nanocomposites. Journal of Applied Polymer Science 116, (2010) 191–202.

[62] Guadagno, L., Naddeo, C., Vittoria, V., Sorrentino, A., Vertuccio, L., Raimondo, M., Tucci, V., De Vivo, B., Lamberti, P., Iannuzzo, G., Calvi, E., Russo, S. Cure Behavior and Physical Properties of Epoxy Resin—Filled with Multiwalled Carbon Nanotubes. Journal of Nanoscience and Nanotechnology 10, (2010) 2686–2693.

[63] Hosur, M., Barua, R., Zainuddin, S., Jeelani, S., Kumar, A., Trovillion, J., Pereza, Y. Processing and characterization of epoxy nanocomposites with Mwcnt's/Cnf's using thinky and 3-roll shear mixing techniques. Matéria (Rio de Janeiro) 15, (2010) 247–253.

[64] Jin, F., Ma, C., Park, S,. Thermal and mechanical interfacial properties of epoxy composites based on functionalized carbon nanotubes. Materials Science and Engineering: A 528, (2011) 8517–8522.

[65] Kim, J., Kim, H., Kim, S., Kathi, J., Rhee, K. 3-Aminopropyltriethoxysilane Effect on Thermal and Mechanical Properties of Multi-walled Carbon Nanotubes Reinforced Epoxy Composites. Journal of Composite Materials 43, (2009) 2533–2541.

[66] Kim, H., Kim, S., Kim, J., Rhee, K., Kathi, J. Thermal and Tensile Properties of Epoxy Nanocomposites Reinforced by Silane-functionalized Multiwalled Carbon Nanotubes. Journal of Macromolecular Science, Part B 49, (2010) 132–142.

[67] Da Silva, W., Ribeiro, H., Neves, J., Calado, H., Garcia, F., Silva, G. Multi-walled carbon nanotubes functionalized with triethylenetetramine as fillers to enhance epoxy dimensional thermal stability. Journal of Thermal Analysis and Calorimetry 115, (2014) 1021–1027.

[68] Prado, L., De La Vega, A., Sumfleth, J., Schulte, K. Noncovalent functionalization of multiwalled and double-walled carbon nanotubes: Positive effect of the filler functionalization on high glass transition temperature epoxy resins. Journal of Polymer Science Part B: Polymer Physics 47, (2009) 1860–1868.

[69] http://xgsciences.com/wp-content/uploads/2012/10/10-15-13_xGnP-M_Data-Sheet.pdf downloaded 6-11-15.

[70] http://asbury.com/Current%20Tech%20Flyers/TF%20TC%20Series.pdf downloaded 6-11-15.

[71] Born, M., Oppenheimer, R. Zur quantentheorie der molekeln (On the Quantum Theory of Molecules (translation by Hettema, H.). Annalen der Physik 389, (1927) 457–484.

[72] Gaussian 09, Revision D.01, Frisch, M. J.; Trucks, G. W.; Schlegel, H. B.; Scuseria, G. E.; Robb, M. A.; Cheeseman, J. R.; Scalmani, G.; Barone, V.; Mennucci, B.; Petersson, G. A.; Nakatsuji, H.; Caricato, M.; Li, X.; Hratchian, H. P.; Izmaylov, A. F.; Bloino, J.; Zheng, G.; Sonnenberg, J. L.; Hada, M.; Ehara, M.; Toyota, K.; Fukuda, R.; Hasegawa, J.; Ishida, M.; Nakajima, T.; Honda, Y.; Kitao, O.; Nakai, H.; Vreven, T.; Montgomery, J. A., Jr.; Peralta, J. E.; Ogliaro, F.; Bearpark, M.; Heyd, J. J.; Brothers, E.; Kudin, K. N.; Staroverov, V. N.; Kobayashi, R.; Normand, J.; Raghavachari, K.; Rendell, A.; Burant, J. C.; Iyengar, S. S.; Tomasi, J.; Cossi, M.; Rega, N.; Millam, M. J.; Klene, M.; Knox, J. E.; Cross, J. B.; Bakken, V.; Adamo, C.; Jaramillo, J.; Gomperts, R.; Stratmann, R. E.; Yazyev, O.; Austin, A. J.; Cammi, R.; Pomelli, C.; Ochterski, J. W.; Martin, R. L.; Morokuma, K.; Zakrzewski, V. G.; Voth, G. A.; Salvador, P.; Dannenberg, J. J.; Dapprich, S.; Daniels, A. D.; Farkas, Ö.; Foresman, J. B.; Ortiz, J. V.; Cioslowski, J.; Fox, D. J. Gaussian, Inc., Wallingford CT, 2009.